

ANTHROPOMETRIC BREAST MOTION SIMULATOR ROBOT FOR BRA EVALUATION

Henry Paul Goodell

A dissertation submitted to the faculty at the University of North Carolina at Chapel Hill in partial fulfillment of the requirements for the degree of Doctor of Philosophy in the Joint UNC/NCSU Department of Biomedical Engineering in the Graduate School.

Chapel Hill
2019

Approved by:

Sharon Joines

Robert Dennis

Kenneth Donnelly

Mark Tommerdahl

© 2019
Henry Paul Goodell
ALL RIGHTS RESERVED

ABSTRACT

GOODELL, HENRY PAUL. Anthropometric Breast Motion Simulator Robot for Bra Evaluation.

(Under the direction of Dr. Sharon Joines and Dr. Robert Dennis).

Within the bra industry there exists a need to quantify fit and performance of test bra designs. While finite element simulation of breast dynamics has been undertaken for imaging and surgical planning, for this real-world application a physical breast simulator with motion control was designed, built, evaluated, and refined through a second iteration. This simulator is based on 3D scans from a professional bra-testing model which were converted into composites of molded-silicone-simulated skin and breast tissue integrated around a SLS 3D printed nylon lattice torso. An initial evaluation of the simulator breast motion was undertaken using standard position and acceleration metrics as well as damped oscillation and rheological studies of various breast formulations. A clinical study of breast firmness and tissue dynamics was completed to validate the simulator formulation and motion as well as to provide a knowledgebase for further improvements and future research inquiries.

Through all time, my love and admiration to my wife Jessica.

ACKNOWLEDGMENTS

The NCSU College of Design Materials Lab is acknowledged for use of their CNC mill and CNC waterjet for several plates. I would also like to acknowledge Byungsoo Kim for assistance during molding of the initial simulator, Catalina Salamanca Mendez for assistance as a design researcher during the clinical study phase, and Warren Ginn of Ginn Design for his assistance with the simulator version 1 housing. I would also like to acknowledge Hanesbrands Inc. for their financial support of this project and continued funding of others.

TABLE OF CONTENTS

LIST OF TABLES	viii
LIST OF FIGURES	ix
CHAPTER 1: FEMALE BREAST TISSUE ANATOMY AND DYNAMICS	1
Introduction.....	1
Anatomy.....	2
Dynamics	2
Problem and Hypothesized Solution.....	3
CHAPTER 2: FEMALE BREAST TORSO AND BREAST PROTOTYPE 1.....	5
3D Scan(s) to Lattice Torso and Outer Mold.....	5
Method of Build.....	13
Material Quantification.....	17
CHAPTER 3: BREAST MOTION SIMULATOR PROTOTYPE 1	22
Mechanics and Method of Build.....	22
Dynamic Quantification.....	27
CHAPTER 4: FEMALE BREAST DYNAMICS AND DUROMETER CLINICAL EVALUATION.....	39
Clinical Study Design	39
Method of Build.....	42
Durometer Quantification and Comparison.....	46
Dynamic Quantification and Comparison	48

CHAPTER 5: FEMALE BREAST, TORSO, AND MOTION SIMULATOR 2.....	61
Design Reasoning and Method of Build.....	61
CHAPTER 6: DISCUSSION AND FUTURE STUDIES	76
Method Development and Insights	76
Future and Ongoing Studies.....	77
APPENDIX A.....	80
APPENDIX B	86
APPENDIX C	87
REFERENCES	88

LIST OF TABLES

Table I	Formulations (1 through 4).....	19
Table II	Formulation Motion Profiles (1 through 3).....	30
Table III	Viscoelastic Analysis of Motion	38
Table IV	Viscoelastic Equations	38
Table V	Oscillatory Analysis of Motion	38
Table VI	Demographic Clinical Study Data.....	47
Table VII	Durometer Clinical Subject Data	48

LIST OF FIGURES

Figure 1	Standing Scan with Breasts and Sans Breasts	7
Figure 2	Torso Scan Lattice Generation	8
Figure 3	Lattice plus mount plus edge reinforcements	10
Figure 4	Breast Mold and Lattice	12
Figure 5	Silicone - Nylon Lattice composite	13
Figure 6	Outer and Inner Surface of Breast Mold	14
Figure 7	Wrinkles and Inner Surface of Breast Mold with Skin Layer	16
Figure 8	Breast Mold and Lattice, Torso Lattice, & Torso Lattice with Breasts	17
Figure 9	Durometer	18
Figure 10	Simulator Formulation Photos (1-4);	20
Figure 11	Durometer Technique	20
Figure 12	Formulation Durometer Data	21
Figure 13	Simulator Version 1 Labview Interface	24
Figure 14	Simulator Version 1 Housing	25
Figure 15	Mechanics of Motion	25
Figure 16	Pneumatic Simulator in Housing (Version 1)	26
Figure 17	Rotational and Vertical Motion Stages	27
Figure 18	Breast Simulator 1 Motion Frame Captures	28
Figure 19	Motion Profiles of Formulations 1 through 3	31
Figure 20	Acceleration Motion Profiles	32
Figure 21	Jerk Motion Profiles	33
Figure 22	Areola-only versus torso-only motion	36

Figure 23	Relative Areola-only Motion Log-decrement Example of Formulations	38
Figure 24	Clinical Study Area	43
Figure 25	GoPro Camera, Blacklights, and Treadmill Setup	44
Figure 26	Raw GoPro 120 FPS Video, 530nm High pass Filtered under Blacklights	45
Figure 27	Durometer Grid Location Numbering	46
Figure 28	Subject 1 Jumping Right Breast	52
Figure 29	Subject 2(4) Jumping Right Breast	53
Figure 30	Subject 3(2) Jumping Left Breast.....	54
Figure 31	Subject 3(6) Running Left Breast.....	55
Figure 32	Subject 4(7) Jumping Right Breast	56
Figure 33	Subject 5(7) Jumping Right Breast	57
Figure 34	Subject 6(4) Jumping Right Breast	58
Figure 35	Subject 7(387) Jumping Left Breast.....	59
Figure 36	Subject 7(389) Jumping Left Breast.....	60
Figure 37	Uniformized Torso	69
Figure 38	Uniformization Length Variations of Lattice	69
Figure 39	Simulator Lattice Version Comparison.....	70
Figure 40	Comparison of Lattices within 3D Scan.....	71
Figure 41	SLS Nylon 3D Printed Mold around Torso.....	71
Figure 42	Representation of Spine within 3D Scan.....	72
Figure 43	Pressure Sensor Tubing Placement (Version 2)	72
Figure 44	Simulator Tubing Management (Version 2)	73
Figure 45	Breast Motion Simulator (Version 2).....	73

Figure 46	Simulator Version 2 in Housing	74
Figure 47	Servo Chain-Coupled Simulator in Housing (Version 2)	74
Figure 48	Hybrid Servo Chain Assembly	75
Figure 49	3-Phase Servo-Rotational Axis Magnetic Mount.....	75

CHAPTER 1: FEMALE BREAST TISSUE ANATOMY AND DYNAMICS

Introduction

Evidence of torso mannequin use for apparel fitting has been documented as early as the ancient Egyptian pharaohs.¹ In apparel manufacture, there have been comparisons between the accuracy of 3D body scanning and anthropometric measurements.²

Anthropometric test devices (ATDs) have been applied in transportation-system testing and simulations beginning over sixty years ago.³ These physical simulators for the human body have been approximated using various material construction.⁴ The utility of ATDs has been proven and validated against human biomechanics.⁵

Finite element simulations have been undertaken not only for ATDs, but also for imaging and surgical planning.⁶⁻¹⁰

Contemporary physical simulators of human female breasts have been used in clinical breast exam (CBE) skills training, using controlled-firmness lumps.¹¹⁻¹² These CBE simulators have proven comparable to live standardized patient simulation training.¹³ For tactile feedback in CBE skills training, a capacitance-based-touch-sensor phantom has been developed.¹⁴ Inductive sensors have also been developed for training clinical-palpation skills.¹⁵

Additionally, breast phantoms have been developed for lightweight breast prosthetics.¹⁶ Others have developed simulations for better post-mastectomy breast prostheses and their possible role in decreasing stigma and improving breast cancer stage-at-presentation in Mexico.¹⁷

Anatomy

These simulators approximate the shape and physical characteristics of the human female torso. A study of breast-tissue anatomy has been undertaken, showing anatomical structure of the skin and gland tissue as well as muscle and fascia.¹⁸ Breast mechanics, elastic modulus, and mechanical properties have also been discussed in regard to the ribcage, tissue, and fascia.¹⁹ Another discussion of breast and surrounding tissues was part of a surgical publication of breast augmentation.²⁰ Human tissue has also previously been quantified using a durometer.²¹ The accuracy of simulators has yet to be thoroughly quantified using this durometer technique.

Dynamics

In apparel design, the human form is the basis for fit, in the form of mannequins or in fitting sessions on human models. Apparel is typically designed in static positions specific to bra fit and relative to a “neutral breast position”. Although the position of the breast is static in the mannequins, “neutral breast position” has been captured through a variety of methods. These methods include submersion in water, air, or oil²²⁻²⁴, as well as dynamic approximation²⁵ using motion dynamics as the breast moves in gravity at 1G vertical acceleration. All these methods attempt to negate gravimetric effects on breast position and shape.

Methods for capturing breast position include measuring changes in position with posture markers, magnetic position sensors,²⁶ Novel Pliance capacitive-based pressure sensors,²⁷ and S2011 Novel Sensors.²⁸ These measures allow for comparisons between neutral positions and the positions generated by bra design.

There have been multiple studies assessing breast motion dynamics. Breast dynamics have been studied during walking and running gait cycles as well as during trunk rotation²⁹. Areolas displacement, sans bra versus with bra, has been researched during both treadmill and

over-ground running.³⁰ Breast motion at different levels of support during exercise has also been examined.²⁷ Changes in the range of motion of the breast over a 5-kilometer run have also been explored.³¹ Breast strain during exercise and the oscillations of the breast after motion at accelerations of over 2G have been studied.³² Strain and acceleration, as well as breast size, have been explored as predictors of breast discomfort.⁴⁴

Breast motion dynamics have also been studied as a mass-spring system³³. While these studies and others³⁴ have relied on breast mass for calculations, we disregard mass mathematically during our studies of breast dynamics because the mass of our formulation versions are roughly equal and not singular masses, but rather complex volumes. This disregard of mass has been done with the understanding that breast size is important to breast dynamics.³⁵

Problem and Hypothesized Solution

Current industry-standard, bra-fit analysis involves human fit models that try on bras, and fit is determined by observation and wearer-qualification of fit. While some have put sensors underneath the bra to determine force, they have not removed the variability of the human wearer.²⁷ The human bra-fit model's anatomy can change with regular weight changes or biological rhythms, such as menstruation, that alter water retention and breast size. These variabilities confound measurement results and do not provide a quantified analysis of bra fit and dynamic function.

For dynamic-motion bra evaluations, most have relied on human models running on treadmills to test breast strain and motion. These examples have relied on human subjects which induce variability into the motion data through inconsistent motion profiles. This motion variability increases deviations and, thus, may prevent the quantification of subtle differences between bra-influenced breast motion. The current standard for bra-fit and dynamic-breast-

motion research is to utilize human subjects, limited as they are by variations not only in their motion profiles, but also in the consistency of their physical anatomy over time and their qualitative sensing of fit.

There exists a need within the bra design and manufacturing industry for a test device to evaluate bra fit and function that provides accurate fit-quantification and precision-motion profiles. The variability of human motion in bra evaluation may be negated through precise servo motion control of an anthropometric simulator. To increase the likelihood of adoption, a simple user interface will provide easy control of this motion-generating actuator(s). To limit the scope of this initial solution development, only vertical and rotational motion will be built, and only vertical motion will be analyzed as it is the predominant motion present during jumping.

A physical form of the bra-fit model will be developed to provide a more standardized form upon which to fit the bras, negating the variability of a single human form. This human form will be appraised by the evaluators to ensure it provides the functionality to conduct bra-fit testing and to ensure it adequately mimics human tissue.

CHAPTER 2: FEMALE TORSO AND BREAST SIMULATOR PROTOTYPE 1

The process of designing and building the breast motion simulator started with 3D scans of the chosen subject, which were then transformed into uniformized surfaces without holes. These scans could be manipulated more easily and thickened into molds. Additionally, these 3D scans were uniformized at a chosen millimeter resolution to produce a mesh able to be transformed into a lattice structure to support the tissue simulants overtop and interface with the mechanics of the rest of the simulator.

3D Scan(s) to Lattice Torso and Outer Mold

Hanesbrands Inc. provided 3D scans of a standard human bra-fit model they regularly utilize for fit evaluation. These 3D scans consisted of multiple scans with holes that had not been combined into a water-tight surface. Initial scan files were fused using HP 3D Scan software (previously named David Scanner) into watertight .obj or .ply files. The provided scans involved multiple positions of the model and breasts, including standing-arms-down, bent-over, and arms-up positions. Each of these scan sets were fused and output to be utilized for original files for mold construction. Although each of these positions caused breast deformations, only the standing-arms-down scan was utilized for lattice production. The molds and analysis of the bent-over and arms-up positions are shown in the appendix. Moving forward, only the standing-arms-down-position scan will be utilized for production of 3D models.

The watertight-3D-file-produced surface consisted of nonuniform meshes. While this nonuniformity provides high levels of detail, it can increase complexity in Boolean operations. The whole-body surfaces were made solid and then digitally plane cut using Meshmixer software

to remove the head, arms, and below the umbilicus to produce a torso-with-breasts file. The cuts of the arms were mirrored across the medial plane of the body and are digitally smoothed while preserving shape by brush-selecting only the areas adjacent to the cuts. The arms-down position prevented accurate capture and rendering of the armpit, so careful smoothing and digital cutting of the arms was undertaken to better represent the armpit after smoothing.

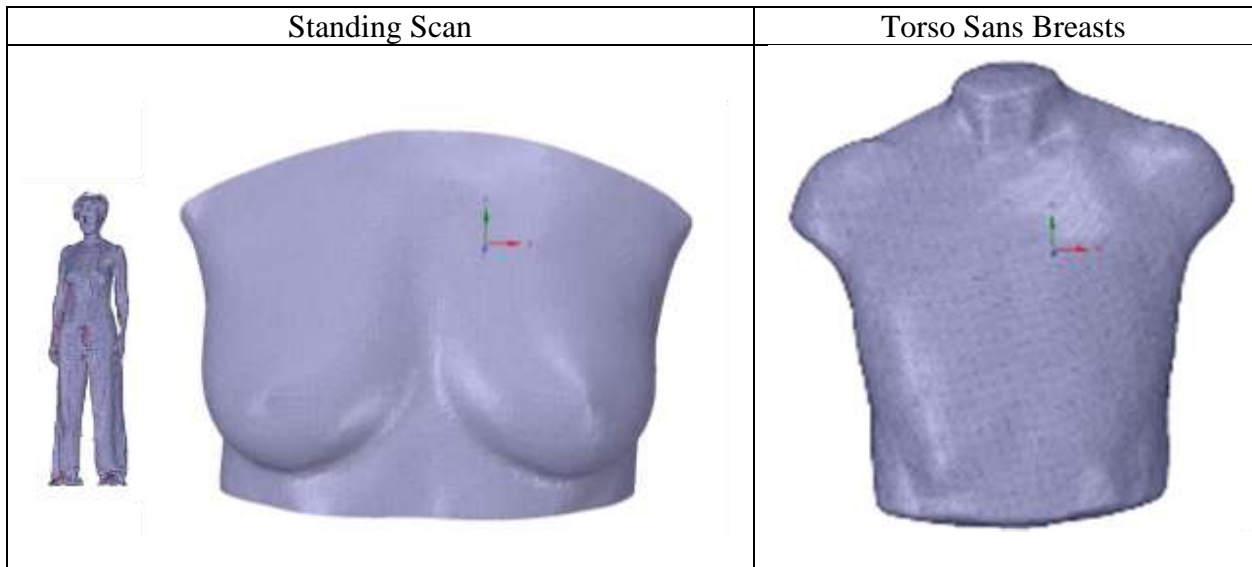
These nonuniform-mesh-torso-with-breasts files have their breasts digitally removed using either a 3D Systems Touch X Haptic device, then smoothed, or via a maximum smooth function in Meshmixer by brush-selection of the breast and the immediately adjacent area. The haptic method works well but is dependent on the user's ability to shave off tissue in a manner that reflects anatomical tissue distributions. The maximum smooth method provides consistent and user-independent, repeatable results and was selected as the method of record moving forward. The only caveat is that sufficient adjacent areas around the breast must be selected to enable full reduction of the breast tissue to a flat surface. Three iterations of smoothing were undertaken to ensure a flat surface; however, other models may require other smoothing iterations or techniques. The resulting nonuniform 3D files were torso without breasts and were used as the basis of the lattice generation.

Figure 1 shows the original whole-body scan, a plane cut section only encompassing the breasts and the torso without breasts. These files represent the basic techniques of conversion of an original scan files into files that can be utilized for mold construction and more complex operations, but only after making the surface-mesh uniform. Mesh uniformization is done using ANSYS Spaceclaim, Meshlab, Autodesk Netfabb, or other software chosen for license availability at the time of use. The whole torso, with or without breasts, was selected for uniformization in lieu of an area-specific selection and variable uniformization parameters.

Using these uniformization parameters (various mesh average lengths) produces different distributions over the torso and breast surfaces. Any detail loss occurs at this operation and could produce suboptimal reproduction of the original 3D scan (and, thus, the real-world object to be reproduced). For molding an exact reproduction, the original high-resolution mesh (or as close as possible) should be utilized versus a less dense mesh after uniformization (used for lattice). In lattice construction, a longer distance between nodes should be used to create larger spaces between the lattice members.

A lattice is used because it decreases the weight of the support structure. Additionally, the lattice may provide functional benefits such as increased flexibility due to its thin members versus a solid construction. Finally, a lattice allows the silicone (in this case) to intercalate, or infiltrate, into the lattice openings and provides stronger attachment between the composite parts (nylon and silicone in this case).

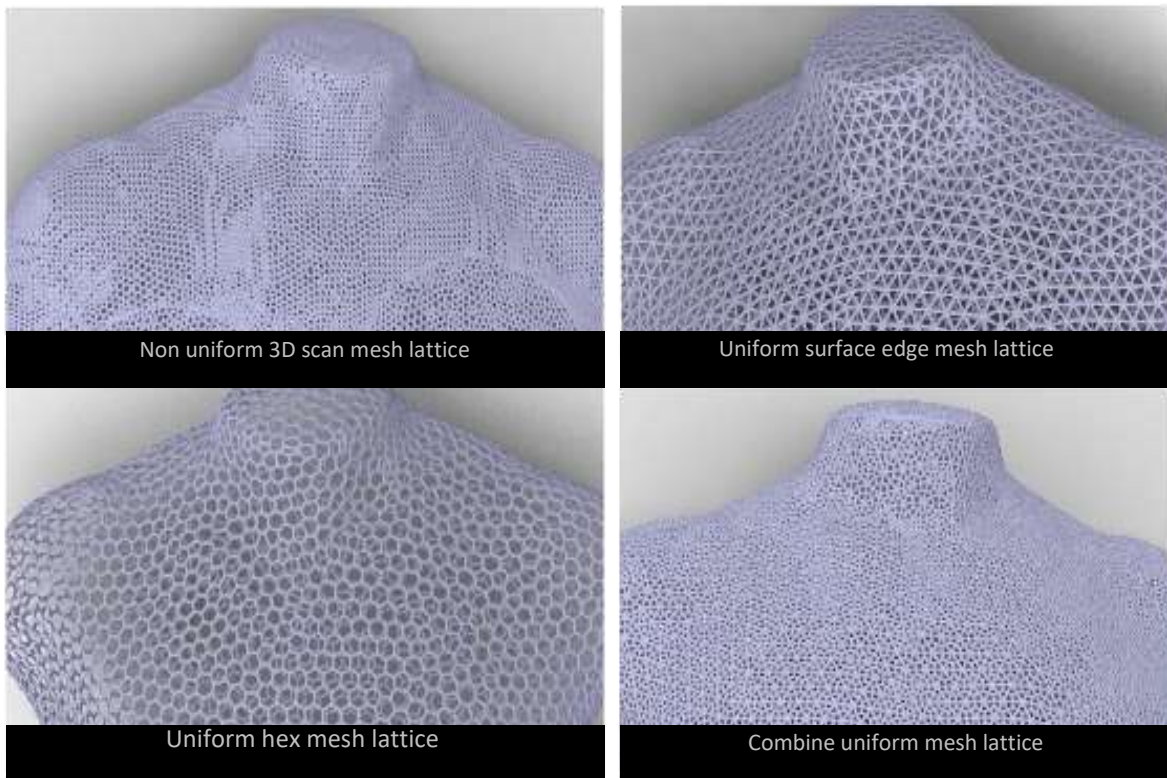
Figure 1. Standing Scan with Breasts and Sans Breasts. (*Partial Torso Test*)



The lattice is constructed using a nTopology Element software with uniform mesh parameters applied before importing. Within this nTopology software, the basic uniform mesh is

imported and converted to a lattice. For this initial version 1 of the simulator, rather than changing the mesh size to change the lattice opening characteristics, a larger mesh size was used, and then two techniques for forming the lattice were combined. These two lattice generation techniques were a hex prism edge and a surface edge rule for mesh generation. The input mesh is either directly thickened to lattice for the surface edge rule, or input mesh nodes are circled or encompassed by hex shapes that have nodes at the center of each surface polygon triangle. These two meshes produce different lattice results as seen in Figure 2.

Figure 2. Torso Scan Lattice Generation.



For this initial prototype of the simulator, these two generated lattices are combined to form the final lattice. Both lattice generation techniques thickened the mesh thickened uniformly at 2mm diameter. Although a linear thickening would have been preferred, this was not available in the free version of the software. Thus, the thickened lattice contained a lattice that was roundly

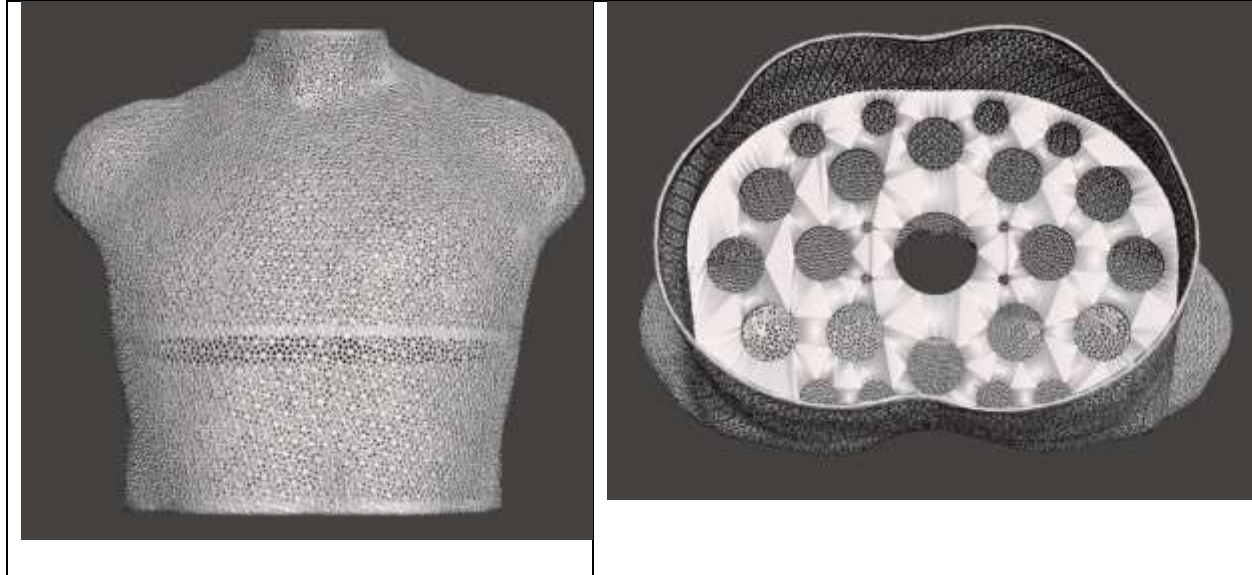
thickened which, in turn, created errors in allowed thicknesses when sent for 3D printing as many aspects/edges did not pass inspection for allowable thickness for the employed printing technique.

After the combined lattice was generated, it was exported into ANSYS Spaceclaim, and a solid transverse plane section was designed (8mm thick) to interface with the simulator mechanics. This 8mm thick piece was located slightly cranially to the level of the areolas. This mount section was Boolean combined with lattice, and two sections at the neck and bottom of the torso were designed by thickening the uniform-torso-sans-breasts-mesh 2mm inwardly. The torso lattice was Boolean combined with the thickened neck and lower torso edge sections, and the resultant lattice-plus-mount-plus-solid sections at the neck and lower torso edge were plane cut to create openings at the neck and bottom of the simulator. These solid sections at the top of the neck and bottom of the torso provided reinforcement to the lattice to minimize the possibility of cracking the relatively delicate lattice. To increase the success rate of Boolean combining of the lattice with the solid sections, lattice export resolution must be optimized to maintain lattice detail without overly growing the file size output. This final combined lattice is shown in Figure 3.

While, in retrospect, combining the hex and surface-edge lattices only differs slightly from simply changing the mesh-uniformization-size parameter, the resulting combined mesh is visually appealing and, more importantly, provides holes within the mesh that are small enough to be sealed. The holes within the mesh are an important aspect of this simulator for two reasons: firstly, the lattice holes decrease the weight of the structure employed (the torso in this case); and secondly, the lattice holes provide a highly-roughened surface for the silicone-tissue simulant to grip onto and into. One requisite aspect of the lattice holes is that the surface tension of the

silicone must allow the silicone to flow into the holes and result in a sealed, watertight torso that may be placed within a mold without allowing leakage of the silicone through the lattice.

Figure 3. Lattice plus mount plus edge reinforcements (*Right: inferior view of mount plate*)



These lattice openings, or holes, must be carefully selected to provide attachment and allow the surface tension of the silicone to bridge the holes and create a continuous watertight, sealed surface. If the holes are too big, bridging over the holes with silicone to create that sealed surface will be difficult. If the holes are too small, the silicone will not sufficiently flow into the holes to create the necessary strong attachment between the silicone tissue and the lattice.

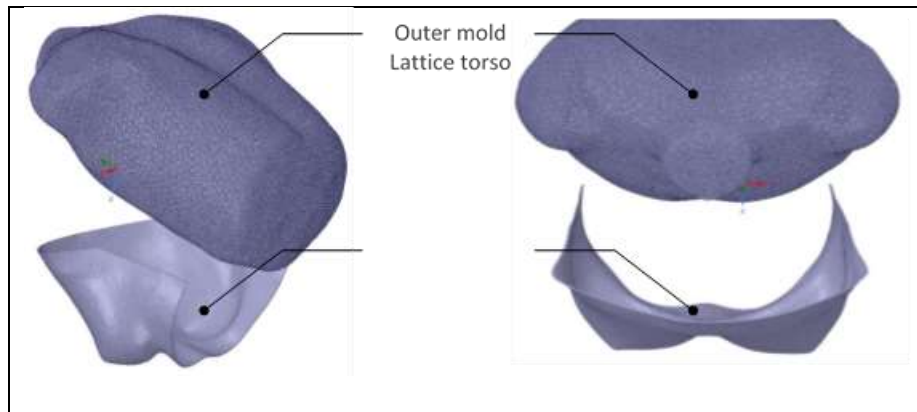
In order to conduct a preliminary test to determine if this silicone-to-lattice attachment would work as intended, a small section of the final design of the lattice was printed, along with a mold, to allow formation of the breasts onto the lattice. The breast mold was designed by thickening the original-torso-with-breasts-3D file outward 2mm and then plane cutting both the lattice with mount and the mold to create a small section for testing the process of molding. Both the lattice and mold were 3D printed using a selective-laser-sintering (SLS) technique for powdered 6/6 nylon due to its strength, flexibility, durability, and availability. The supplier,

Shapeways, Inc., was chosen since the printing footprint of 300mmx300mmx500mm provided a large enough printing volume using this SLS technique to produce the lattice as a single-part print. Before uploading the final lattice torso, the file size was minimized to the vendor's upload limitation by simplification with Meshlab software, using quadratic edge decimation.

The basic method of breast mold to the torso is shown in Figure 4, and the resultant successful test is shown in Figure 5. The thickened breast mold has side sections that effectively wrap around the sides of the lattice, encompassing the sides of the breast tissue. This mold is then fastened to the lattice with either bungee cables or extra-large binder clips (2-inch), as in the case of this test section of the lattice and breast mold. The breast tissue formulation used in this initial test was an all-parts Ecoflex 00-30 which, while grossly too firm for anthropometric tissue simulation, provides easier molding for this partial torso test piece. The resulting breasts attached thoroughly to the lattice, were removable for remolding, though not effortlessly, and, after an initial layer of silicone was applied to the lattice to make it watertight, prevented large amounts of silicone leakage through the lattice while molding. The attachment of the mold to the lattice occurred without difficulty. Although exact alignment of the breast mold to the lattice was lackluster, it was decidedly functional for this initial prototype.

This ~2mm thickness for the mold was found to flex to a degree deemed non-beneficial to reproduction of exact dimensionality of the original 3D scan, and there was concern that such a thin SLS printed surface may tend to warp during printing. A simple addition of rib-type reinforcements may help mitigate warping, but these were not integrated into this version of the simulator lattice or molds. While bending or flexibility may in some situations be considered beneficial (e.g. mold release), bending may be decidedly nonoptimal in other situations (e.g. molding).

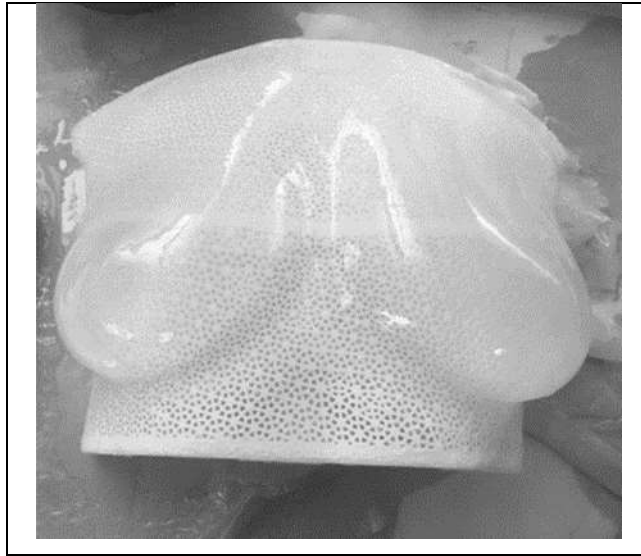
Figure 4. Breast Mold and Lattice (*top*); Torso Lattice (*Bottom Left*); Torso Lattice with Breasts (*Bottom Right*);



The rigid outer mold and lattice were aligned and mounted together with binder clips and bungee cords. The 2mm lattice was also thickened bilaterally instead of inwardly, resulting in a 1mm outward error of the mold. Additionally, the sealing of the mold resulted in some offset error. Additional dimensional error came from applying the initial watertight silicone layer on top of the lattice before applying the outer mold. This molding error would later be approximated using a comparison of the original 3D scan with a photogrammetry 3D scan of the final version 1 (not shown).

A 3D print of the full-torso-lattice (version 1) prototype was ordered from Shapeways, Inc. using SLS 6/6 nylon. The same breast mold was used since it covered the full breast tissue volume, attached well to the lattice, and the additional cost of new molds was deemed nonbeneficial. Breast molds for 3D scans in different positions were designed and ordered in SLS nylon from Shapeways, Inc., and datasets and photos of varying positions are shown in the appendix.

Figure 5. Silicone – Nylon Lattice composite. (*Partial Torso Test*)



Method of Build

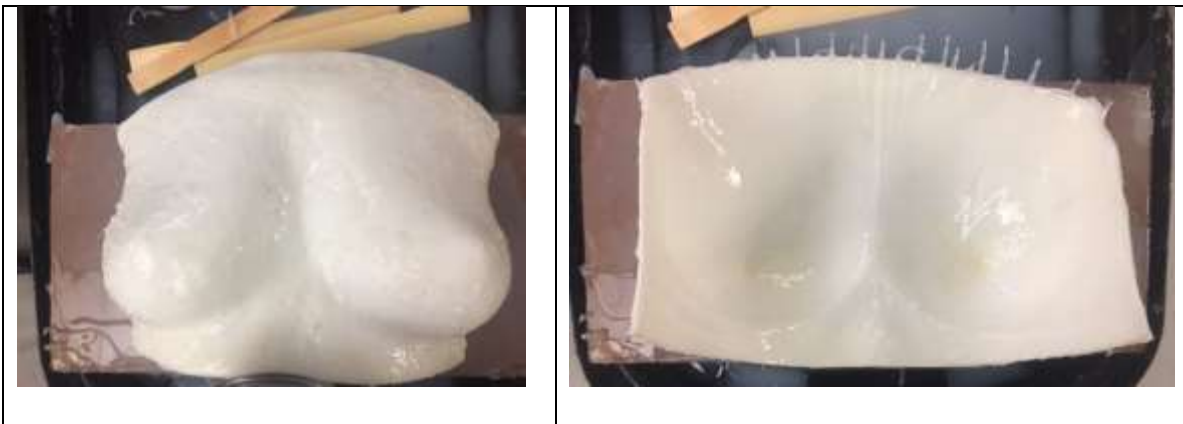
The process of using the breast mold to form and attach the breasts onto the lattice torso was explored, and it was found that a 00-10 silicone skin layer over a silicone gel (penetration 8 to 15cm) produced breasts that were the most qualified to mimic human breasts. Before molding, the lattice torso was made watertight through application of 00-10 Ecoflex silicone. This silicone layer intercalated into the pores and holes of the lattice while flowing under surface tension, giving the lattice a watertight surface. Each SLS printed breast mold was sealed with XTC-3D by Smooth-On (diluted with ethanol or acetone) and allowed to cure overnight. These sealed molds were then coated with a thin layer of melted Sonite Wax (Smooth-On) applied with a brush. This sealing process can impart a small inward dimensional error as it offsets the inner surface of the molds by up to 1mm. Sealing and waxing facilitates release of the silicone and eases removal of excess silicone from the molds.

To these sealed molds, five layers of 00-10 silicone was applied to the inner surface and allowed to drip off under gravity and surface tension, creating layers of thin silicone. Each layer

was allowed three to four hours to set between applying the next layer. These layers generally summed up to approximately a 1.5mm of simulated skin layer thickness (data not shown).

Anatomical skin thickness and elasticity has previously been discussed and supports the chosen thickness¹⁹, which suggests that changing this layer elasticity and thickness may better simulate the aging breast.³⁶

Figure 6. Outer Surface of Breast Mold (*Left*); Inner Surface of Breast Mold with Skin Layer (*Right*);



These skin layers were established on the outer mold before connecting this skin thickness to the watertight torso. Before attachment, two FEP sheets were applied to the superior aspect of the inner surface of the breast skin layer on the breast mold, preventing adhesion of the top of the breast skin to the watertight lattice, which allows access to the breast cavity following attachment of the skin to the torso. The skin was attached to the torso through application of silicone and/or silicone gel to the inner surface of the skin and to the outer surface of the torso.

Silicone was applied between the breast skin and the torso, the mold was secured to the torso with bungee cords and binder clips around the lower edge, and time was allowed for curing. The mold was tilted to prevent pooling of silicone in the volume of the breast. After curing, the FEP sheets were removed, and the silicone gel was degassed and poured into the

breast cavity carefully to prevent bubbles. After curing, the mold was gently peeled away, starting at the edges.

Care is required when peeling the silicone off the inner surface of the mold during the process of attachment. Figure 7 shows the resulting wrinkles in the silicone when poorly released of the silicone from the mold. Also shown is the resulting sag caused by air pockets that developed during molding, preventing proper adhesion between silicone layers. Also reflected is the process of removing the breasts to reuse the lattice for a new breast molding, by which one gets under and then pulls the watertight layer of silicone off and out of the lattice.

The intercalation of the silicone into the lattice to make it watertight produces a layer of silicone that, because of surface tension, forms a texture much like a “popcorn ceiling” in a house, in which, because of the surface tension of the silicone, the silicone flows into the lattice pores only partially to create a watertight layer over the lattice. In addition to sealing the lattice before introduction into the mold, this watertight layer over the lattice allows easier removal of the mass of silicone skin and tissue for remolding as shown in Figure 7.

The final watertight torso is shown in Figure 8 along with the final torso with breasts attached. A 3D photogrammetry scan of the final torso with breasts was compared to the original-3D-torso-with-breasts file using Cloud Compare software (data not shown). Greater error was present at the edge where the breast mold attached to the watertight torso. The errors in lattice, both due to the watertight seal and the bilateral lattice generation, combined with the breast-skin offset contributed to over-error in the molding process. The error was most evident at the top of the chest where the breast tissue was backfilled after attachment.

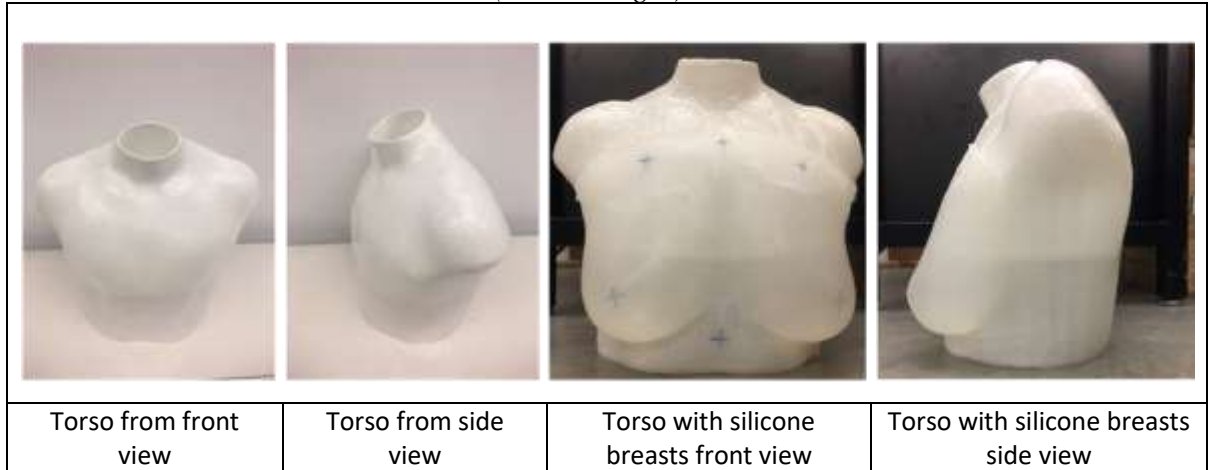
Figure 7. Wrinkles (*Left*); Inner Surface of Breast Mold with Skin Layer (*Right*);



While this initial version proved satisfactory for initial testing, the overall molding process needed improvement. Initial stakeholder and end-user evaluations did not point out molding errors but suggested improving breast tissue firmness, making it softer and more closely resembling human breast characteristics. The lattice was found to be susceptible to moderate cracking, which was subsequently repaired, at areas adjacent to the mount plate. While evaluators generally liked the lattice, this fragility necessitated increasing the thickness of the lattice in the later versions.

Additional 3D scans of the professional human model in other positions such as standing, arms up, and bent 90 degrees at the waist were turned into breast molds by thickening outward 2mm using Netfabb and printed in SLS nylon using Shapeways, Inc. (shown in appendix). These additional molds and breast shapes proved disadvantageous. The standing position was the only breast mold used to study various material formulations of the breast tissue simulants.

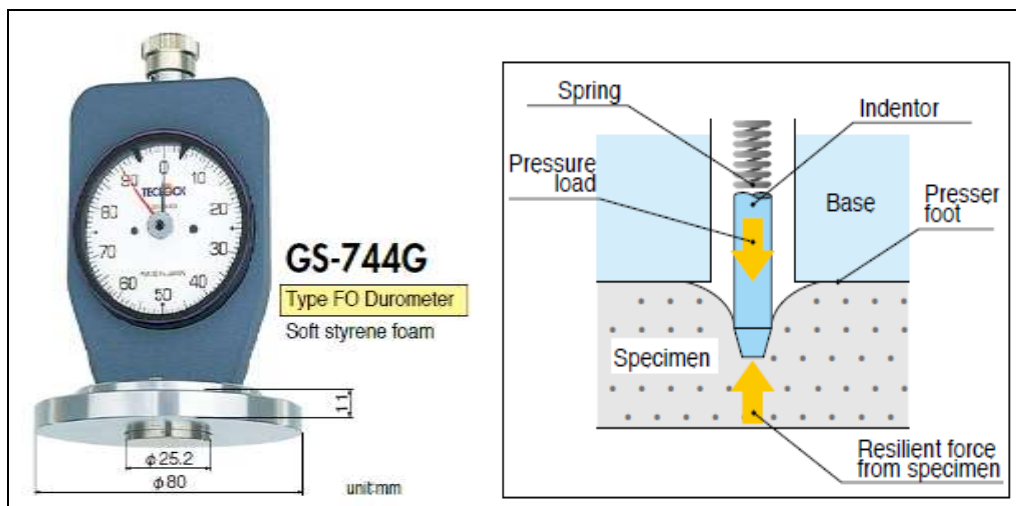
Figure 8. Breast Mold and Lattice (*top*); Torso Lattice (*Bottom Left*); Torso Lattice with Breasts (*Bottom Right*);



Material Quantification

Mechanical imaging of the breast has previously been undertaken using cots devices.³⁹ FO-type durometer measurements of foam and human tissue demonstrate the range of measurements expected for human tissue.²¹ A FO-type durometer (GS-744G) shown in Figure 9 consists of an indenter applied with a known force, in this case a spring, to the surface of the material to be tested, producing a measured displacement corresponding to the durometer reading in this range. These ranges are from zero to one hundred on this durometer with a smaller number corresponding to a lower durometer or firmness of the material. This durometer scale (FO) provides anthropometrics for breast tissue firmness without the need for elastography approaches, either through mechanical imaging,⁴⁰ ultrasound-based,⁴¹⁻⁴² or other modalities.⁴³ Initial measurements of human breast firmness confirm that this technique, and the range of the firmness of the breast simulator, are within the physiologic range.

Figure 9. Durometer (from manufacturer datasheet);



While the silicone skin (Ecoflex 00-10) was maintained at a 1:1 volume ratio of parts A:B and with three layers of thickness in an attempt to lower the firmness of the breast tissue, the ratio of these parts was varied in the breast tissue simulant. Table 1 shows the ratios of 1, 1.05, 1.1, or 1.2-part A to 1-part B by weight of Qgel 317 silicone gel breast tissue simulant, labeled as formulations 1 through 4. These ratios were chosen after consulting the manufacturer, which suggested up to 1.1:1, and initial tests of range of crosslinking at various ratios. The 1.2:1 ratio produced an extreme viscosity qualitatively near, but qualitatively still more viscous, than any single part alone.

Figure 10 shows photos of each of formulation (1 through 4). While formulations 1 through 3 had progressively more wrinkles and sagging as the ratio of the breast tissue simulant moved away from 1:1, each of these formulations maintained structural integrity and was a good replication of the intended mold form. Formulation 4 was excluded from further quantitative evaluation because it was deemed too soft and deformed too greatly under gravity. Formulation 4 was also prone to ripping. Long term (six months or more), all formulations but formulation 1 were prone to propagation of small rips in the skin causing fragility and the ultimate breakdown

of the simulators. In the short term, formulations 1 through 3 were deemed acceptable and were used for further mechanical quantitative evaluation.

TABLE I. FORMULATIONS (1 THROUGH 4)

	Formulation 1		Formulation 2	
	Skin	Breast tissue	Skin	Breast tissue
Material	EcoFlex 00-10	Qgel 317	EcoFlex 00-10	Qgel 317
Ratio	A:B=1:1	A:B=1:1	A:B=1:1	A:B=1.05:1
Layers	3 layers		3 layers	-
	Formulation 3		Formulation 4	
	Skin	Breast tissue	Skin	Breast tissue
Material	EcoFlex 00-10	Qgel 317	EcoFlex 00-10	Qgel 317
Ratio	A:B=1:1	A:B=1.1:1	A:B=1:1	A:B=1.2:1
Layers	3 layers	-	3 layers	-

This durometer was used to measure firmness at nine locations in an approximate square 3-by-3 inch grid pattern (1-inch² per location) centered on the areolas and including immediately adjacent areas as shown in Figure 11. The firmness measurements were made while the simulator was in the supine position with the durometer maintaining a vertical position relative to gravity (normal) as shown in Figure 11. A pillow was placed under each shoulder to maintain normal position of the durometer while measuring lateral or medial portions of the grid. Each measurement was made in triplicate and averaged.

Figure 12 shows the durometer data for formulations 1 through 3. Three formulations were evaluated, all with the same skin formulation (three layers of 1:1 00-10 silicone), each with different ratios of silicone-gel-breast-tissue simulant at ratios of silicone gel parts A:B of 1:1 (Formulation 1), 1.05:1 (Formulation 2), and 1.1:1 (Formulation 3). As the ratio of part A of the silicone-gel-breast-tissue simulant increased, the relative crosslinking of the silicone gel decreased (part B contains the catalyst). As the relative catalyst decreased, the silicone became

more fluid and less gel-like while showing less durometer firmness. Results in Figure 12 show that as crosslinking was decreased from the 1:1 formulation, the firmness also decreased.

Figure 10. Simulator Formulation Photos (1-4);

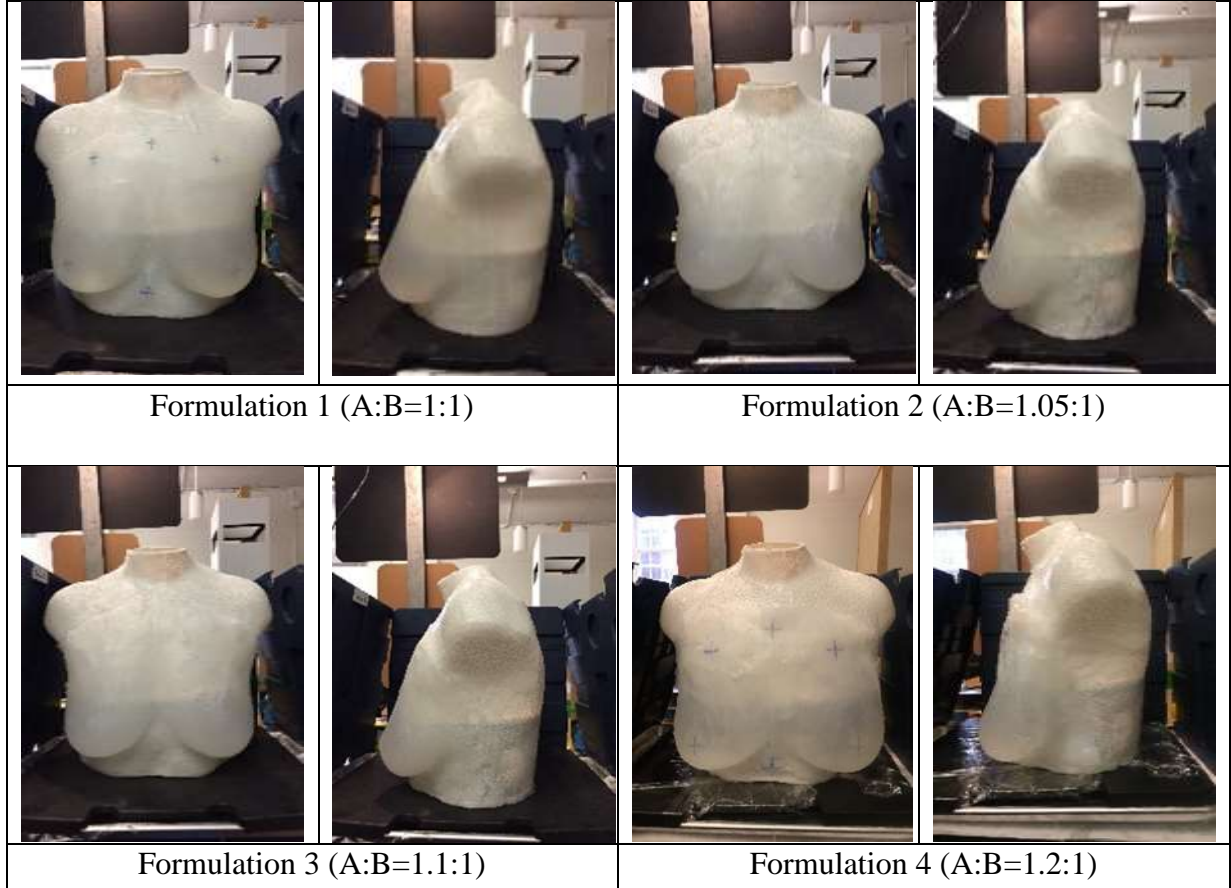
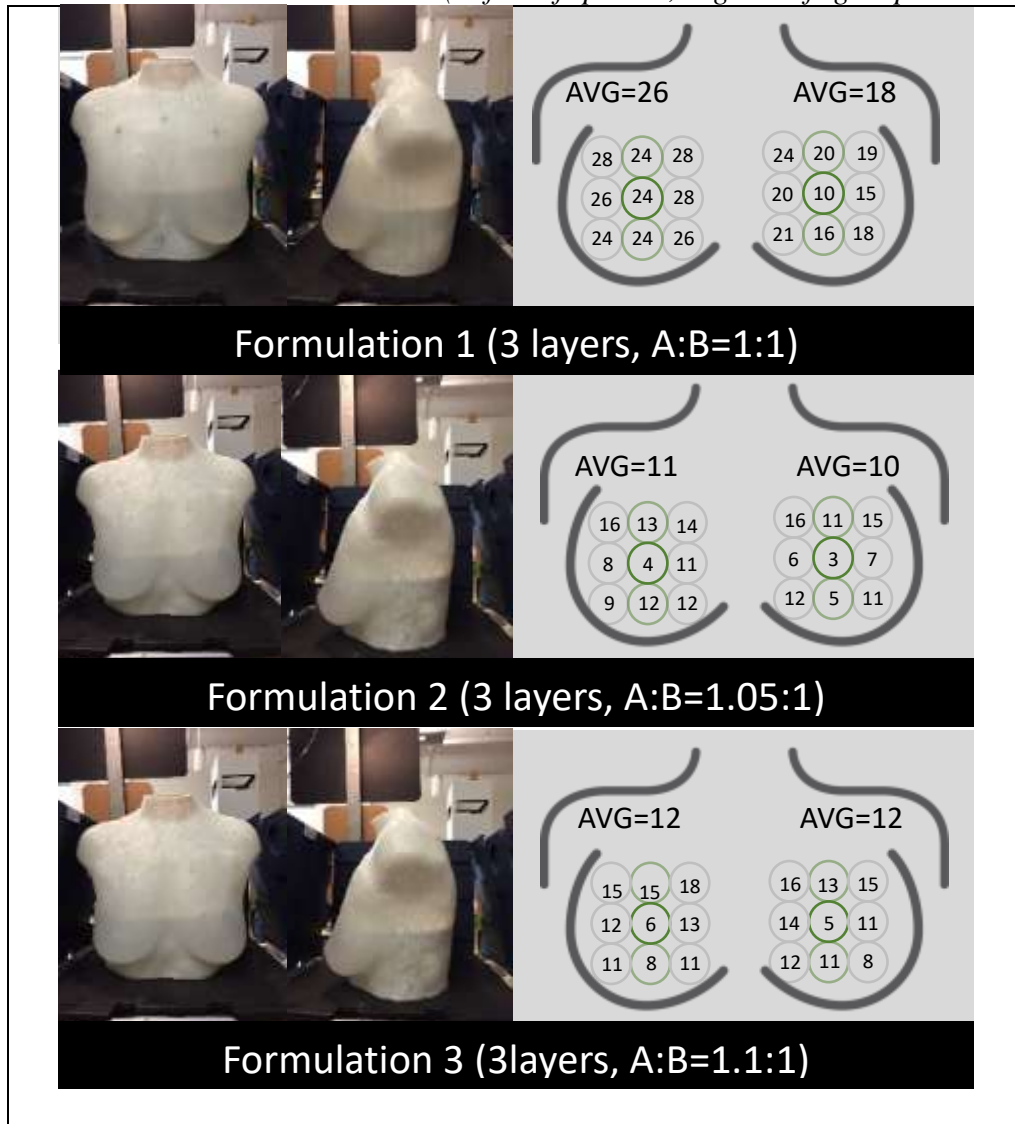


Figure 11. Durometer Technique (Left: location placement, Middle: torso tilting for normal durometer, Right: grid of measurement locations);



While the durometer measurements between formulation 1 and formulation 2 were different, formulations 2 and 3 were not different; this may be due to a maximal softness being attained or a lack of precision or accuracy from the durometer. Although the standard deviation values are not shown here for simplicity, common variations among durometer readings can vary widely. At low durometer readings (e.g. below 10), the durometer measurements can easily vary by 5 points, while above 15 to 20, the reading can vary by 10. The average of the standard deviations of each individual location durometer measurements is 2.0 on the FO scale.

Figure 12. Formulation Durometer Data (Left-half: photos, Right-half: grid pattern and data)



CHAPTER 3: BREAST MOTION SIMULATOR PROTOTYPE 1

There exists a need not only to evaluate the mechanical properties of the breast simulator, but also the dynamics of the breast simulator under anthropometric, or physiologic, conditions of running (or walking) for future evaluation of bra designs. Currently, Scurr and other researchers evaluate breast movement utilizing live human bra models running on treadmills and various motion capture techniques. The torso lattice has been designed and built to directly connect to the mechanics of the rotational and vertical motion stages of the simulator. For this initial prototype, pneumatics was chosen to ensure enough force was provided to the detriment of point-by-point precision of vertical motion.

Mechanics and Method of Build

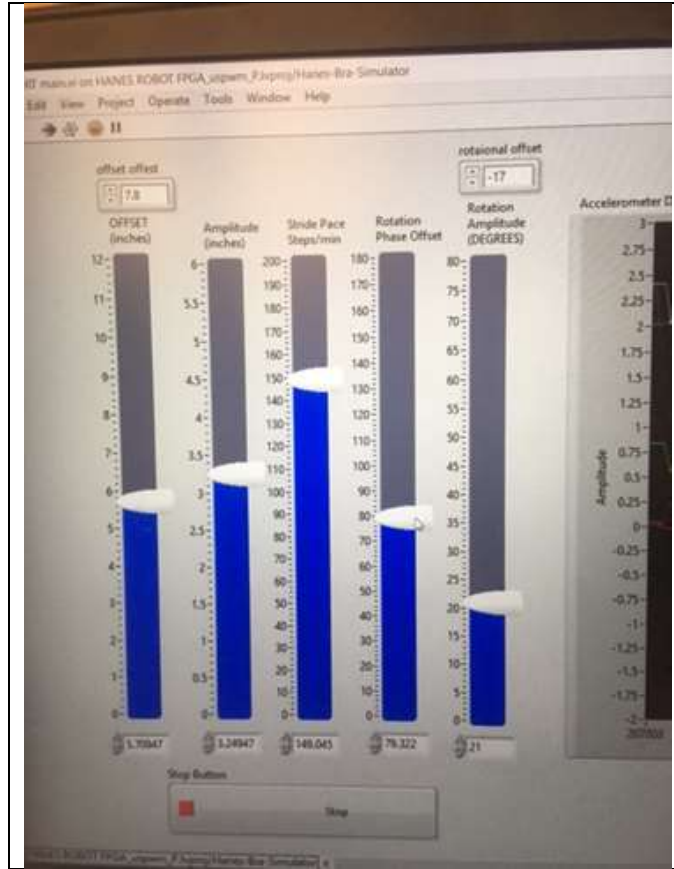
Figure 14 shows the enclosure (housing) formed from 80/20 aluminum extrusion, 2-inch by 2-inch, connected at the corners by dual anchor nut inserts CNC milled into the ends. The housing is divided into two primary areas by a 1-inch PVC plate attached mid-height with the 80/20 frame dividing the housing into two sections. The lower section houses a vertical sheet of 1-inch PVC onto which attaches the torso's vertical actuator assembly, controller, air supply, and power. The upper section provides physical access to the torso and is enclosed with polycarbonate doors for safety.

Figure 14 shows the DC servo assembly that provided the rotational motion for the torso. The servo plate assembly, atop the air cylinder, provided support for the servo and servo shaft bearing, and attachment for the pull-wire potentiometer. This assembly contained a DC Servo motor (RMCS-2257, previous servo shown) operating at 900RPM coupled to an Actobotics

Servo Hub Shaft through a ½”-bore pillow block. Attached atop the hub shaft is a custom aluminum angled plate which fitted into a corresponding aluminum block attached to the bottom of the 3D-printed-lattice-torso-mount plate; this allowed attachment of the lattice torso to the motion actuator via a hand-tightened ¼” bolt accessed through the neck of the torso. This single bolt attachment, milling operation, underpowered rotation servo, and poor planar rigidity of the rotational stage proved disadvantageous, and all were subsequently replaced in the second version of the simulator.

As shown in Figure 15, this servo assembly was mounted to the top plate of a double acting, non-rotating NFPA tie double rod air cylinder (McMaster-Carr, 2.5 inch bore) providing 12 inches of vertical motion and preventing rotation of the air cylinder. Feedback control of the cylinder position was provided through a pull-wire potentiometer connected between the air cylinder ends. Pneumatics were controlled through a Festo MPYE-5-3/8 proportional valve controlled by a MyRIO board and custom Labview program. Figure 13 shows the front panel of the Labview program and control parameters. While the FPGA program provided the servo feedback and spline generation, the ARM processor provided the user interface and communication through FIFO buffers with the FPGA. The front panel shown was locally run on a computer but was mirrored on the ARM and simply provided user input control of the ARM program. While this project used direct USB connections, it is possible to log into the MyRIO over wifi at lowered speeds. Wireless sensor arrays in subsequent versions and crowded wifi environments limited the utilization of wireless communication. While PID control was possible for slower speeds, it was deemed disadvantageous at higher speeds. A timed program for square wave proportional valve actuation was chosen.

Figure 13. Simulator Version 1 Labview Interface

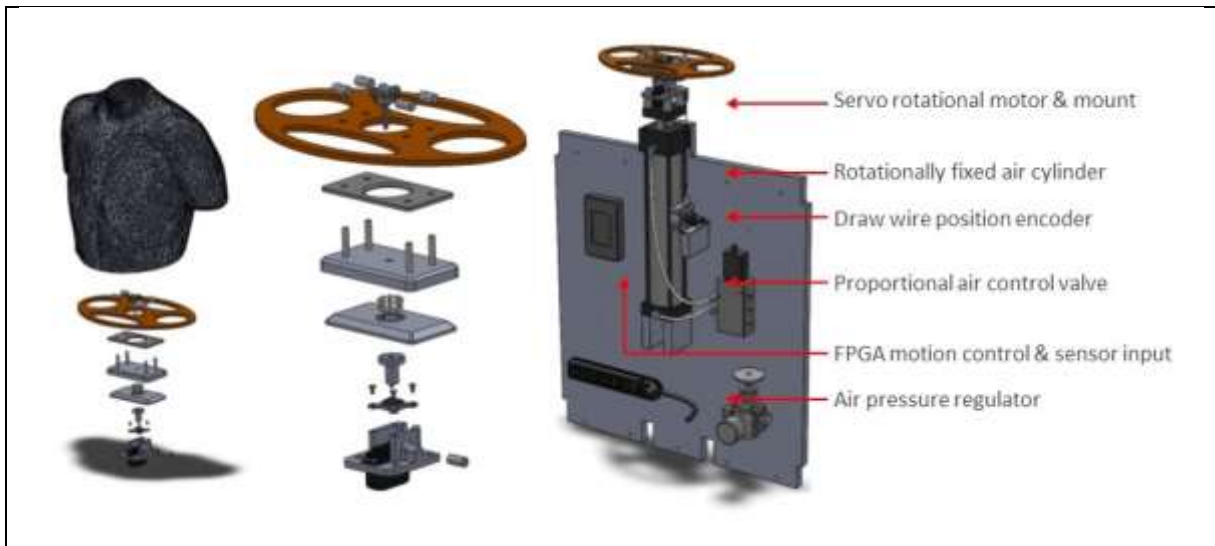


Although the pneumatic valve provided large acceleration (up to 6G), the compressibility of air, pull wire resolution and timing limitations, feedback control timing limitations, valve control limitations, and a general lack of point-by-point control necessitated that the vertical motion system be switched to a more rigidly-coupled mechanism in the second simulator version. Due to the pneumatics, this version can be thought of as a force – or stress – controlled device rather than a more rigidly coupled, positionally controlled device. Another limitation of this system is that the dual tie rod air cylinder exhibits a very slight wobble with the torso atop it while moving. This wobble is most obvious on the narrow axis of the tie rods, meaning the wobble is greatest along the axis through the two tie rods as the lateral stability is lessened by the lack of width at this base.

Figure 14. Simulator Version 1 Housing (*Left: whole, Middle: doors open, Right: photo*)



Figure 15. Mechanics of Motion (*Left: torso with mount, Middle: torso mount to pillow block to servo, Right: air cylinder and vertical plate housing pneumatic controls*)



Initial tests used a square wave motion profile to minimize servo feedback errors through the pneumatics. Figure 16 shows a screen capture from an initial rotation and vertical motion

profile; this video is available upon request. Initially, it was thought that accelerometers placed mid-sternum and at the areolas could provide some motion quantification; however, this proved difficult to implement and standardize. Thus, motion capture alone and vertical motion alone were used for this initial evaluation to limit confounding factors and error.

Figure 16. Pneumatic Simulator in Housing (Version 1)

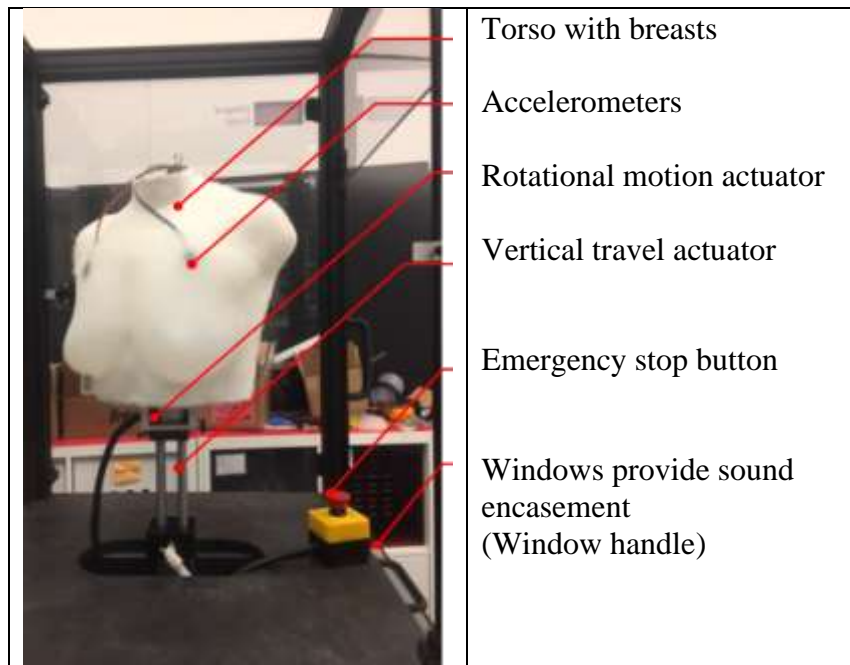
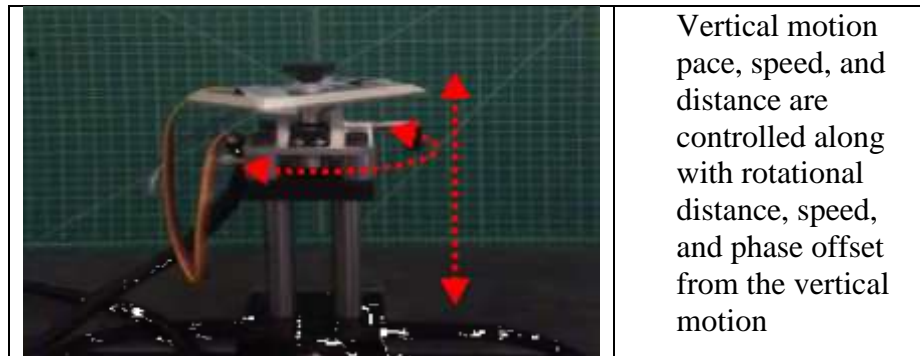


Figure 17 also shows the servo rotational and vertical motion directions. The wide aspect of the dual-tie-rod-air cylinder was placed so that the lateral aspect of the torso is supported. This prevented side-to-side motion, but the weight of the breast tissue overhung the narrow aspect of the air cylinder. The speed of the rotational motion and the undersized servo motor was also a barrier to fully implementing rotational motion concurrently with vertical motion. As the motion capture system used in this initial simulator version was limited to a single camera on plane with the simulator, rotational motion would have induced error in the motion tracking measurements.

Figure 17. Rotational and Vertical Motion Stages (Version 1)



Vertical motion pace, speed, and distance are controlled along with rotational distance, speed, and phase offset from the vertical motion

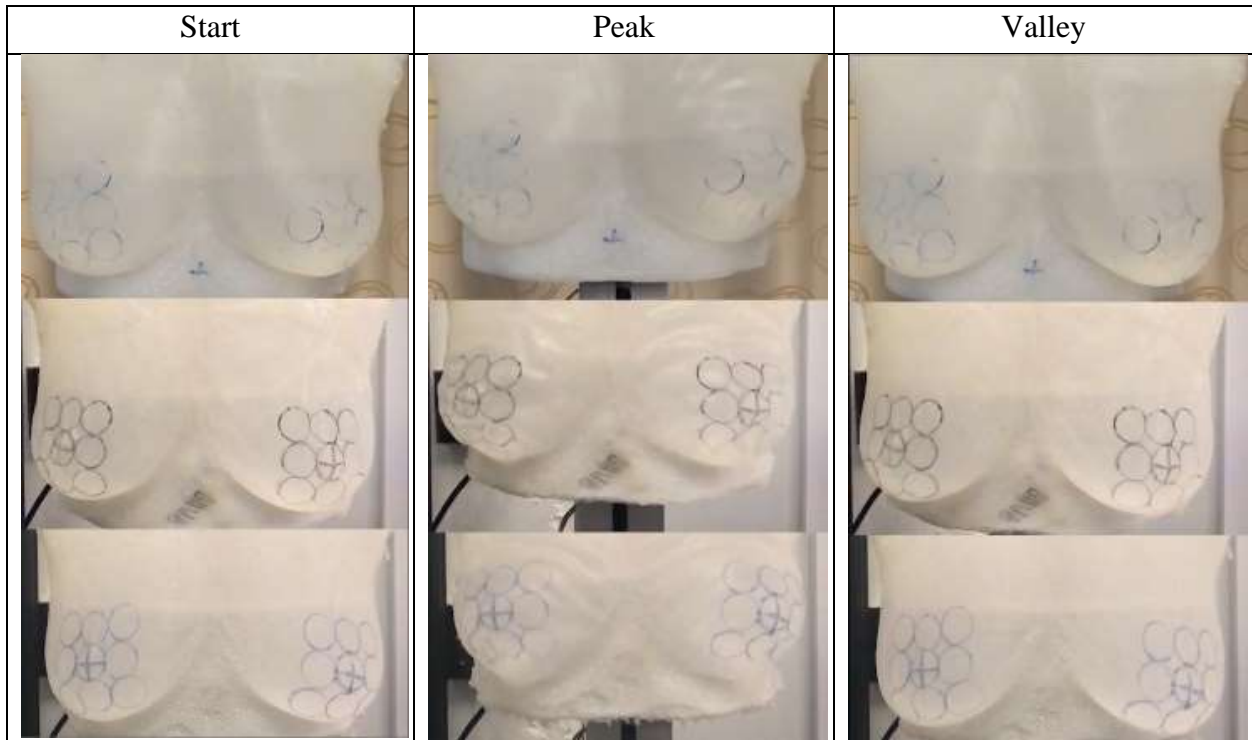
Dynamic Quantification

Simulator 1 motion capture utilized a single GoPro Hero 4 (Peau Productions 72 distortion free lens) at 120fps 1080p. These files were imported into physlets.org Tracker software rather than a multi-camera digital image correlation such as MultiDIC Matlab software toolbox⁴⁰, or other commercial products such as GOM Correlate or SynthEyes software. This method proved slower than other software packages but was accessible and acceptable for this 1D motion evaluation as our cameras were on-plane with the principal vertical motion. Vertical motion was chosen since it simplifies analysis and minimizes confounding motions. While more accurate reproductions of running and other locomotion require more complex motions, we negate lateral and other more complex motions. These more complex anthropometric motion profiles may provide better anthropometric motion simulation and will be evaluated through future iterations of this breast motion simulator. Additionally, more complex non-linear motion profiles outside the current simulator's workspace or range-of-motion may be explored through future parallel cable, or actuator, robotic configurations.

Figure 18 shows motion capture of the three formations at start (or rest), moving through the initial peak (or maximum) of the motion profile, and, finally, at the valley (or minimum) of

the motion cycle. The motion of the areolas relative to the torso shows the torso moves vertically and then returns to its initial position. This final return to rest after vertical motion causes the areolas to overshoot and descend slightly below the static initial resting position of the areolas relative to the torso. Also evident is the wrinkling of the breast skin tissue simulant through the upward motion.

Figure 18. Breast Simulator 1 Motion Frame Captures (*Top: formulation 1, Middle: formulation 2, Bottom: formulation 3*)



Motion tracking of torso markers, midline at the sternal angle and inferiorly, provides vertical displacement of the torso lattice. Markers over the areolas are tracked as the motion profile of the breast plus torso. The torso motion is subtracted from the areolas' markers to get the areola-only motion relative to the torso. While this point-based areola motion is not as

thorough as a 3D scan of the breast during motion, there have previously been finite element analyses of breast motion that more thoroughly explore complex breast motion. This study is meant to be a simple analysis of breast simulator motion to attempt correlation of this motion with formulation and firmness analysis.

Others have used motion outside of the neutral position as a metric of breast motion. For simplicity in this study, we use the static position of the silicone breast composite under gravity as the baseline for our analysis rather than the approximated neutral position of the breast at 0G upward acceleration (1G gravity downward minus 1G upward acceleration). We also simplify our analysis by only examining vertical motion in this study, although rotational and combined motion are currently being investigated further.

Changes in areola-only range-of-motion, as shown in Table 2, reflect a decrease in crosslinking of the breast-tissue-simulant silicone gel. The ratio of areola-only to body-only motion, or percent strain, increases in formulation C as breast tissue crosslinking is at its least. This least crosslinked formulation 3 has the greatest total strain, but the valley is as large as the 1:1 formulation. We use the static breast position at 1G as zero rather than the inferred neutral position of the breast at 0G. This resting gravity acceleration confounds the valley of the breast motion as the resting areolas positions of formulations 2 and 3 are lower than in formulation 1. This may show that, at static gravity, the less firm breast has greater motion in the upward direction than in the downward direction due to its static position under gravity load. These less crosslinked silicones also do not hold their molded shape and confound motion.

Figure 19 shows the motion profiles of the formulations using the pneumatic based vertical motion of simulator 1. The lack of moment-by-moment positional accuracy control of the pneumatic system is demonstrated in the motion path profile, shown in blue. The density of

silicone gel ratios are approximately equal, so the final weights of all test formulations are considered the same (within the error of the molding process). At the same force of motion, the inertial and viscoelastic changes in the formulations confound the motion of simulator 1, producing nearly 5cm in formulation 3 compared to 4cm in formulation 1.

TABLE II. FORMULATION MOTION PROFILES

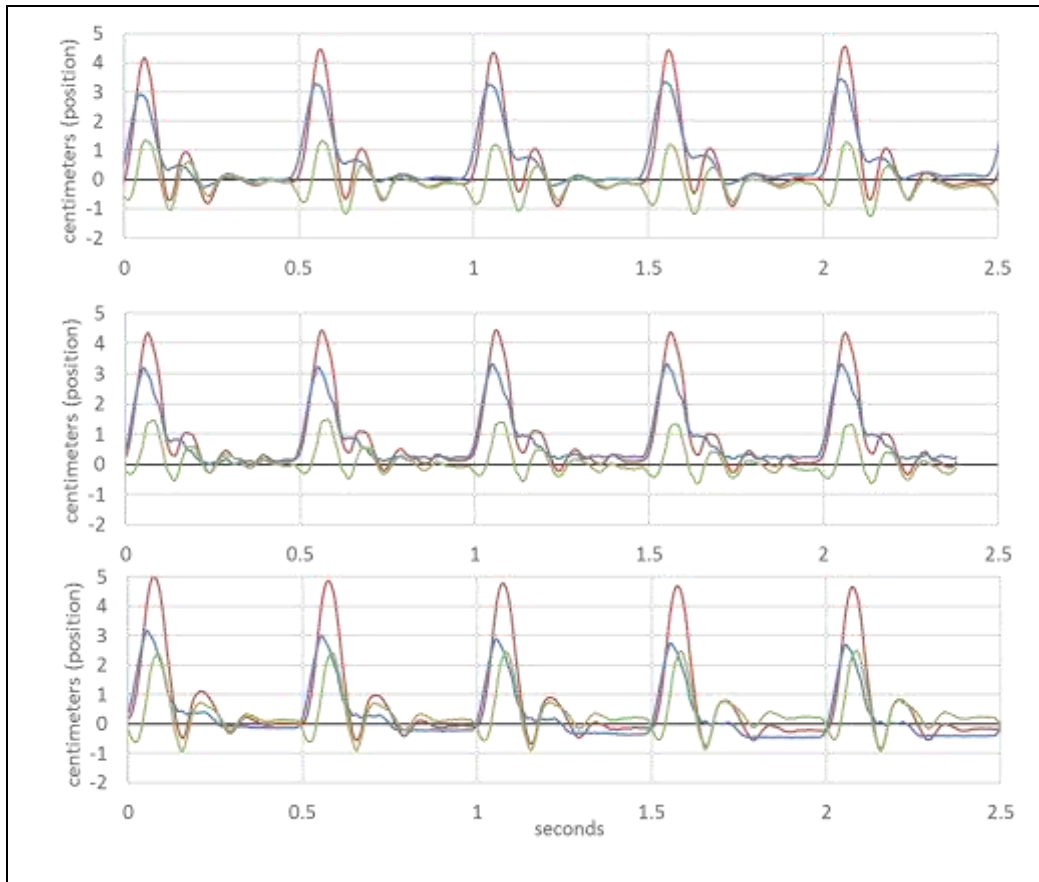
Formulation	Vertical Displacements (cm)		Ratio Areolas/Body Motion (% strain)
	Peak Maximum Average (stdev)	Valley Minimum Average (stdev)	
1	1.16 (0.13)	-1.25 (0.14)	69.8%
2	1.39 (0.07)	-0.55 (0.06)	64%
3	2.46 (0.03)	-0.88 (0.03)	102.6%

The motion of the pneumatic breast motion simulator torso is shown in Figure 19 along with the combined areola-plus-body and areola-only relative motion. The torso-only motion shows the limitation of the pneumatic control, compressibility of air under the load of the torso composite, and the subsequent under-damped control of the first simulator version overall. This aspect of the pneumatics control tends to dampen the actuated motion. Even though the pneumatic actuator is limited in its point-by-point servo positional control, it provides some level of force control through the proportional valve and a good deal of absolute positional control of motion endpoints. Hence, there is a need for a more rigidly coupled, servo-based, second simulator, but the simulator used here provides adequate force and positional control for initial testing.

Figure 19 shows the downward lag in relative motion of the areolas in response to the upward motion of the torso, upward relative overshoot of the areolas at the peak of motion, and subsequent relative undershoot of the areolas when the torso returns to start position. The areolas' oscillations outside of zero position, upon returning to static resting 1G gravity, are also

reflected in the damping of the torso motion as it approaches its resting position. This is an aspect of the pneumatics and force control limitations of the simulator system. While controlling force may more closely approximate human motion, it provides a limitation to quantification and control of position using this simulator system.

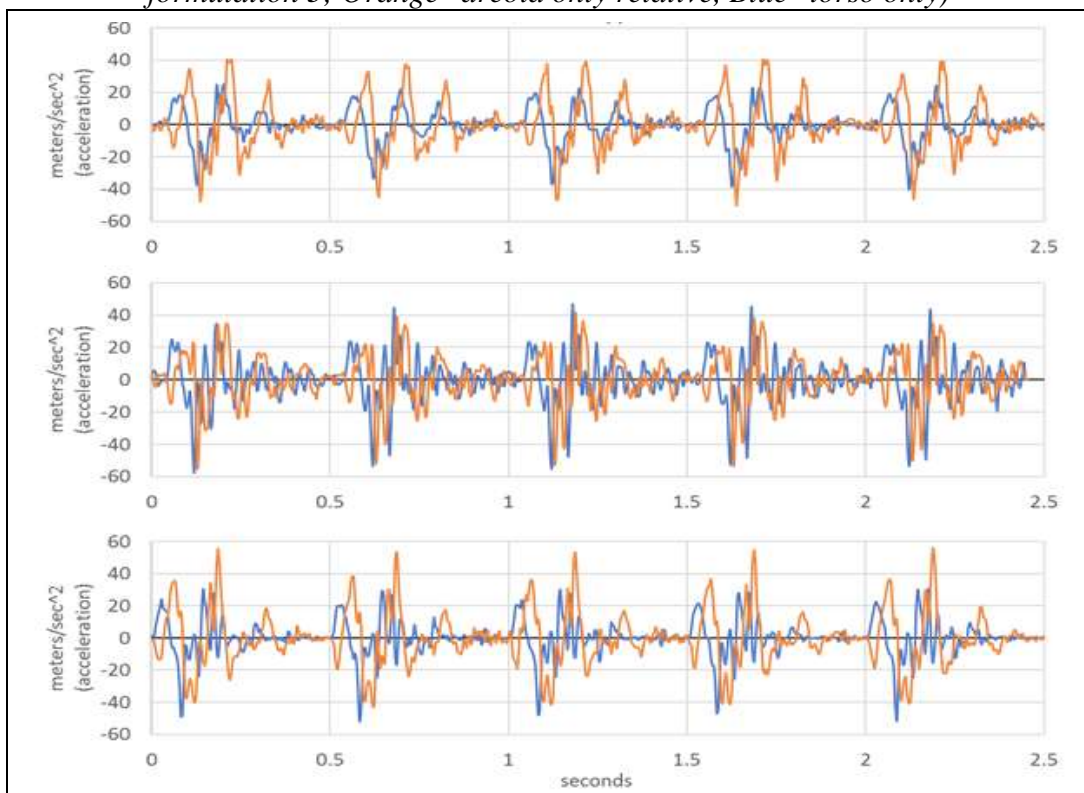
Figure 19. Motion Profiles of Formulations 1 through 3 (*Top: formulations 1, Middle: formulation 2, Bottom: formulation 3; Traces: Red=areola+torso, Blue=torso only, Green=areola only relative*)



Acceleration and strain have been used as predictors of breast discomfort.⁴⁴ Figure 20 shows torso accelerations at 2G and relative areolas accelerations of 4G and up to nearly 6G. The greatest relative accelerations of the areolas occur at the peak and valley of the motion cycle. Formulation 1 shows how the standard 1:1 ratio of the breast tissue formulation produces oscillations that are very consistent and smoother than other formulations. Formulation 1 has a

better form, producing breasts that are firmer and extend slightly further forward from the torso than other formulations. Formulation 3 shows acceleration peaks that are much greater than the other formulations, suggesting the greater relative motion of this less firm formulation. Formulation 2 data is not as smooth as the other datasets. Overall, all torso accelerations were very similar between the formulations despite the damped motion caused by the pneumatics and inertia of the breast tissue mass.

Figure 20. Acceleration Motion Profile (Top: formulations 1, Middle: formulations 2, Bottom: formulation 3; Orange=areola only relative, Blue=torso only)

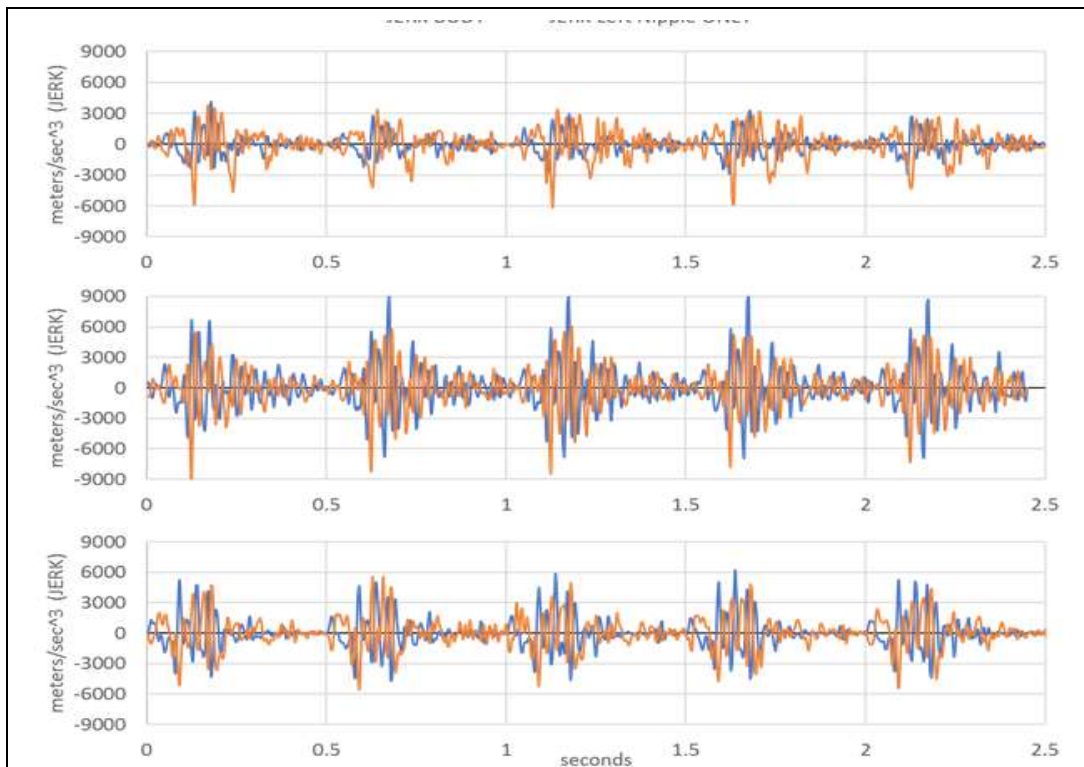


PID feedback of the current Festo valve proved disadvantageous for rigid coupling in vertical travel as shown in these acceleration motion profiles. As the various formulations had nearly identical mass, their accelerations oscillated and varied due to changes in their viscoelasticity, viscous and other losses, and breast mass inertia during motion were confounded

with the compressibility of the pneumatics. These aspects of motion using this pneumatic simulator created error in the overall motion analysis as equivalent forces applied to different simulators produced slightly different speeds of motion and overall positional control accuracy.

The influence of jerk, the derivative of acceleration, on perceived motion strength has been evaluated on the UTIAS Flight Research Simulator.⁴⁵ While jerk, the change in acceleration, has not been explored greatly, it could provide a better evaluation of pain. Jerk peaks of areolas relative motion shown in Figure 21 approach extremes 9000 m/s³. These extremes of areolas relative jerk correspond to the peak and valley of the torso motion profile.

Figure 21. Jerk Motion Profile (*Top: formulations 1, Middle: formulations 2, Bottom: formulation 3; Orange=areola only relative, Blue=torso only*)



The elastic modulus of human breast tissues has been previously discussed.¹⁹ Breast motion is represented in these studies as a single system defined by the areola-only motion. For

these studies we ignored: 1) the mass of the simulator or total mass of the breast tissue since parts A and B are approximately the same mass; and 2) inertial-based aspects of motion. In lieu of more thorough analysis, these assumptions were made to produce a simplified representation of viscous and elastic components of motion as phase angles. The viscous component of damping would be expected to increase with velocity, while inertial aspects of motion would be expected to increase with acceleration.

As stress was applied vertically in this study, the resulting strain in the breast tissue and areolas was delayed. The lag between the torso and areola-only motion can also be viewed as a phase angle between their respective motions. When this phase angle is 0° , the material was considered purely elastic, while it was considered purely viscous at 90° . Although this simulator was not considered a rheometer, these metrics were utilized to better explore strain and viscoelasticity.

Table 3 shows calculations of time lag – and the motion phase angle derived from it – for the areola as the torso moved upward (valley), and overshoot of the areola as the torso moved downward (peak). Figure 22 shows the area of areola lagging the torso, followed by the catch-up phase, and then the overshoot of the areola back to neutral position. Area of motion increased as crosslinking and elasticity decreased and the viscous component increased. The one notable aspect was again the starting position of the breast at 1G gravity; this gravity force pulled the less firm, and more viscous, formulations downward and limited their downward motion during the motion cycle.

As the 1:1 A:B silicone gel ratio is lessened, decreasing crosslinking, the initial valley time lag increased. In table 3 the lag and phase angle are shown. The 1:1 A:B gel had a longer initial lag time – possibly because the shape of the breast was better maintained with this more

rigid formulation. The peak lag time generally increased as the crosslinking decreased, suggesting greater motion due to viscous and/or inertial components. As the crosslinking decreased in the gel, it became more viscous and less elastic, and the firmness decreased as previously shown.

TABLE III. VISCOELASTIC ANALYSIS OF MOTION

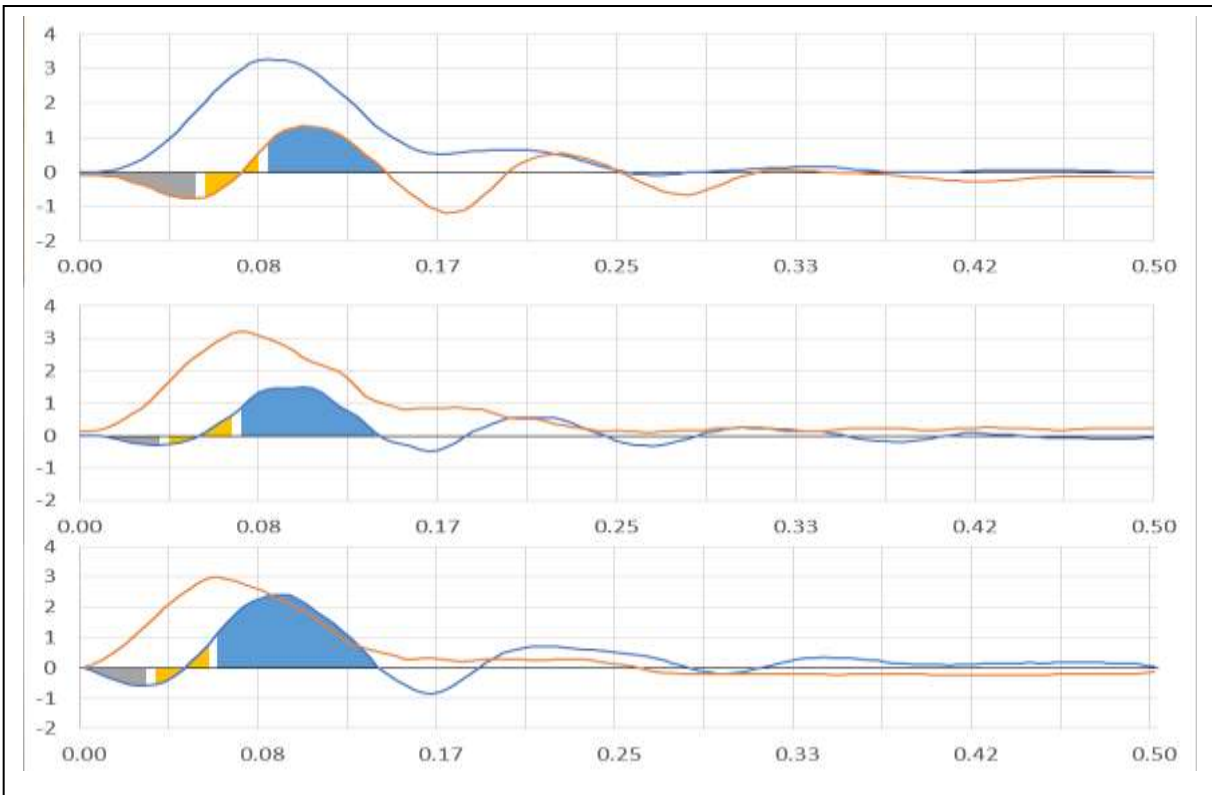
Formulation		<i>Lag Sec (stdev)</i>	<i>Phase Angle (stdev)</i>
A	<i>Valley Average (stdev)</i>	0.048 (0.004)	52.10° (4.09)
	<i>Peak Average (stdev)</i>	0.016 (0.003)	17.60° (2.72)
B	<i>Valley Average (stdev)</i>	0.035 (0.002)	43.65° (2.97)
	<i>Peak Average (stdev)</i>	0.029 (0)*	35.95° (0)*
C	<i>Valley Average (stdev)</i>	0.031 (0.005)	44.62° (7.68)
	<i>Peak Average (stdev)</i>	0.029 (0.002)	41.96° (3.20)

*Standard deviation of time lag less than 0.001 seconds or degrees.

The limitations of the pneumatic actuator were evident as forces from the actuator motion, along with air compressibility, prevented a rigid positional control. The inertia of the breast tissue mass and pendulum motion upon returning to rest impart force into the vertical actuator and modulate its motion and negatively impact positional accuracy. The breast motion simulator did, however, provide excellent standard deviations over the sixteen cycles analyzed for this dataset. The valley time lag of formulation 1 shows a larger lag than any of the other formulations and may be due to the breasts keeping their form better and not initially sagging as much at rest. The more elastic nature of the 1:1 ratio is further shown in the much lower peak time delay as the breast tissue did not overshoot for as long and more quickly returned to

downward motion following acceleration reversal compared to other formulations. The increased speed and slight overshoot of the positional control of formulation 3 confounds this analysis as the percent strain and cyclic timing are changed slightly which may account for the phase angle changes with approximate equal timing. This limitation of the pneumatic system design and control will be changed in subsequent versions.

Figure 22. Areola-only versus torso-only motion; centimeters vertical axis versus seconds horizontal axis (*Upper: formulation 1, Middle: formulation 2, Bottom: formulation 3; Shaded Areas: gray=lag, yellow=catch-up, blue=overshoot*)



The initial areola lag and overshoot at the peak are presented in terms of viscoelasticity; however, they invariably have inertial components as the initial lag (shaded in grey) is the mass of the breast at rest transitioning into motion, while the overshoot (shaded in blue) contains the momentum of the breast in motion overshooting the peak of the torso motion (shaded in yellow). As the mass between the breasts is approximately equal within the limitations of the molding

process, as weights of parts A and B are approximately equal, mass is excluded in favor of this viscoelastic approximation.

What is also noticeable is the oscillation of the areolas-only motion relative to the torso upon returning to resting or starting position of motion. These oscillatory aspects are further explored using basic log decrement of the portion of the motion profile after the breast tissue has been put into motion, meaning the initial valley lag portion is excluded due to inertia. The overshoot at the peak is also excluded and only areolas-only relative motion after the torso returns to rest is analyzed as oscillatory motion. Three representative traces are illustrated in Figure 23, reflecting: 1) the peak; 2) the return to starting position; and 3) the subsequent oscillation of the breast tissue. Formulation 1 is shown in blue, formulation 2 in red, and formulation 3 in green. What is striking is the well-defined oscillatory motion of the areolas relative to the torso.

Table 4 shows the analysis of the oscillatory motion of the areola after the peak of the torso motion. This analysis is a gross simplification of the breast as a single system defined by the areola-only motion, which treats the oscillation of the areola through this final motion as a damped oscillation – like a spring. The compressibility of simulator 1 pneumatics confounds this data and create an under-damped system. Log decrement (1) of the ratio of sixteen sets of successive peaks provides a simplified understanding of the damping of the breast motion simulator formulations as shown in table 4. The damping ratio (2) was derived using the log decrement. Figure 23 also shows representative areola oscillations from the three formulations during three unique oscillations. This analysis shows the damping ratio increasing as the formulation moves away from 1:1, thus relating the crosslinking of the silicone gel with this factor.

Figure 23. Relative Areola-only Motion Log-decrement Example of Formulations.
 (Formulations: blue=1, red=2, green=3)

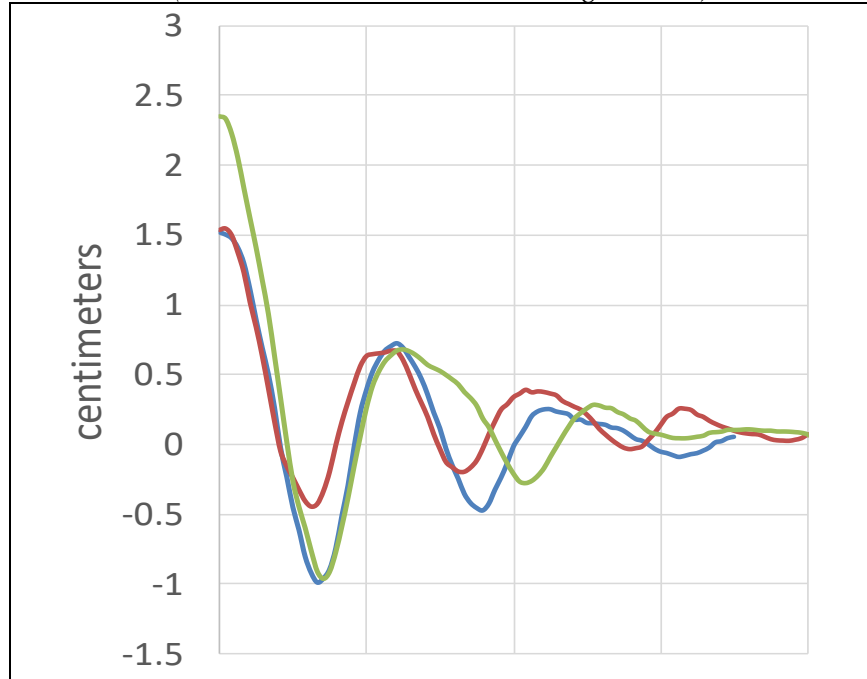


TABLE IV. VISCOELASTIC EQUATIONS

$\delta = \frac{1}{n} \ln \frac{x(t)}{x(t = nt)}$	Log Decrement (equation 1)
$\zeta = \frac{1}{\sqrt{1 + \left(\frac{2\pi}{\delta}\right)^2}}$	Damping Ratio (equation 2)

TABLE V. OSCILLATORY ANALYSIS OF MOTION

	Log Decrement (stdev)	Damping Ratio (stdev)
A	0.7400 (0.00002)	0.1170 (0.0000)*
B	0.8315 (0.0025)	0.1312 (0.0004)
C	1.2412 (0.0009)	0.1938 (0.0001)
*Standard deviation less than 0.00001.		

CHAPTER 4: FEMALE BREAST DYNAMICS AND DUROMETER CLINICAL EVALUATION

IRB approval (#12059) was gained prior to conducting this research study on NCSU campus. A female clinical research assistant was utilized to help with data collection to ensure comfort of the study subject and ease of collection.

Clinical Study Design

Only women with self-reported bra sizes 32 to 34 B, C, or D, along with healthy breast histories, and a body mass index between 18.5 and 30.0 were eligible for participation. The study subject signed a consent form after being provided: 1) a brief verbal description of the study; and then 2) a more in-depth written consent and study description. After the subject's questions were answered and the consent form had been signed, a copy of the consent form was provided to the study subject. The subject was then reminded that she could stop participation at any time without risk. Monetary reward was provided to all subjects who began the study, and no subjects ended the study before completion.

Demographic information, self-reported bra size, and bust and torso measurements were recorded on a paper-based data collection sheet. The research assistant measured (using a flexible cloth tape measure) and recorded the subject's clothed torso and bust-line circumference. Additionally, age group was recorded.

The study was conducted in a screened-off corner of the research area to ensure the subject's privacy. A disposable drape was placed over the examination table and pillow. The subject then removed all clothes above the umbilicus and put on a disposable paper vest. The

research assistant, gloved in disposable non-latex gloves, then assisted the subject into a supine position on the examination table. The research assistant then replaced the removable side-rails to ensure the subject's safety. The subject then exposed each breast, and durometer readings were taken over a 3-by-3 grid centered over the areolas. After all readings were recorded, the subject removed any oils from their torso and breasts using a sanitizing towelette. The durometer was cleaned by the research assistant using sanitizing towelettes before and after each subject. The research assistant placed the pillow under the right side of the subject's torso for the right grid column readings and under the left side of the subject's torso for the left grid column readings using the durometer. Center grid column readings did not require pillow placement. The durometer was used to measure nine locations in a 3-by-3 grid on each breast with three measurements taken at each location. Thus, a total of twenty-seven measurements were taken per breast.

Next, helping the subject to a seated position, the research assistant provided gel-based, removable, disposable pasties (with position markers on the outside), and the subject placed one over the center of each areola. Originally, the markers on these pasties were based on fluorescent paint but were changed to fluorescent vinyl for uniformity. Additionally, markers were placed over the breast surface area as well as midline on the torso and under the breasts. These additional markers were created using either fluorescent paint or vinyl placed onto a skin-compatible, double-sided adhesive tape used for ECG electrodes. After undertaking the motion capture portion of the study, all pasties and electrode tape markers were removed by the subject and discarded. The subject was then offered sanitizing towelettes to clean any residual adhesive remaining on the skin.

To ensure anonymity, the subject was also offered: 1) a face covering (balaclava); and 2) either paper tape (designed to go on the skin) or make-up to cover any tattoos or other identifying marks/scars during the motion capture portion of the study. The research assistant provided aid in applying the coverings as needed. If the subject declined to cover her face or identifying marks, the identifiers were digitally removed.

After all position markers were in place and tattoos/marks/scars covered, the subject removed the paper vest, placed UV safety glasses over her eyes for protection from the blacklights, and stepped onto the treadmill. The treadmill had been covered in fluorescent tape to aid in visibility during the study and to maximize safety. The video cameras were then switched on, and the subject was able to monitor the recording in real-time on a closed-circuit video monitor placed on the treadmill. The cameras had been positioned to minimize the visibility of the subject's face. Room light was then minimized, and the blacklights were turned on to enhance the fluorescence of the position markers on the breasts and improve visibility and contrast of the markers on the video. The video cameras had red (530nm high pass) filters over the lenses to selectively capture the position markers. This aspect of the study minimized subject face or tissue capture and maximized privacy.

Once the subject was comfortable and in the correct location, the video capture began, and the subject was instructed to jump in place three times. This was repeated at least three times while producing separate video files for each set of three jumps.

After jumping, the subject was asked to run in place while three separate ten second videos were recorded. Following jumping and running in place, the subject was asked to switch on the treadmill and slowly increase the speed until their footsteps match a metronome set to 150 beats per minute (BPM) which equates to a running pace. Once a running pace was achieved,

video recording began, and three separate videos of approximately ten seconds each were documented. After completing the running portion, the video cameras and treadmill were turned off. After the treadmill had stopped, the subject exited the treadmill while the research assistant stood nearby if aid was required.

This was the close of the study portion, and the research assistant provided the subject with sanitizing towelettes before leaving the study area while the subject removed the position markers and any coverings, cleaned any residual adhesive from her skin, and got dressed. All markers, sanitizing towelettes, pillow and table coverings, gloves, paper gowns, and tape coverings were then discarded. The subject was paid at this time. Had a subject chosen to quit the study early, she would have been paid at the time she chose to quit. All primary data was kept locked in a secure location offline.

Method of Build

As shown in Figure 24, the clinical study area was separated from the surrounding space by opaque curtains. Within this space, a massage table, with arm rails added for safety, was situated. A screened-off changing area was situated in the back-right corner, allowing research subjects to change in privacy. In the forefront was a treadmill covered in fluorescent tape for safety in low lighting.

Before the motion capture began, the lights were turned off throughout the clinical study area and entire room, and the blacklights were turned on. When the blacklights were on, all persons in the study area were required to wear UV protective glasses out of an overabundance of safety. Once the lights were turned off, the blacklights were turned on, and the safety equipment was in place, motion capture could begin.

As shown in Figure 25, two GoPro cameras were mounted via aluminum GoPro holders to an OpenPartBuildStore 20mm-by-20mm aluminum extrusion, each at an angle of 25 degrees towards the center. Also shown is the real-time monitor of the GoPro video, blacklights, and the metronome that was set to 150 beats per minute for syncing running speed between participants. The safety fluorescent tape on the arms of the treadmill is also visible.

Figure 24. Clinical Study Area (*Above: lights on, Below: blacklights on and lights off*)



On the GoPro Hero 4 with non-distortion 72 degree lens, the Protune feature was enabled and frames per second set to 120. Within Protune the white balance was set to native, the shutter was set to 1/240 seconds, and ISO was set to 800 (or 400). The two GoPro cameras were triggered simultaneously using a CamDo brand Bullet backpack trigger for the GoPro Hero 4.

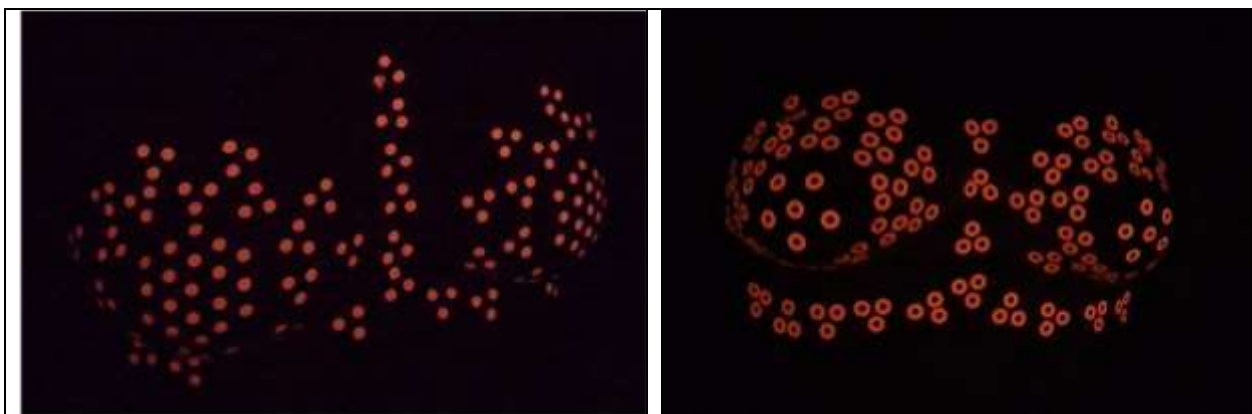
This Bullet trigger allowed the two GoPros to trigger recording and end recording at the same time. This trigger is a software-defined trigger, not a hardware-type, closed-contract or TTL trigger. This causes small propagation errors in the software execution of the trigger signal translate into frame count and timing errors. This aspect of these triggers was one of the biggest challenges of this system and was exacerbated by voltage levels through the system. Combined with the rolling shutter of the GoPro cameras, all causing slight capture errors, there was no post-process able used to satisfactorily match frames within the chosen software. These frame count, start time, and rolling shutter errors limited the ability of this system to properly calibrate at high speed in software such as GOM Correlate. While calibrations were shown to be possible, subsequent stereoscopic motion analysis was replaced by a similar single camera motion analysis similar to the first simulator analysis. The cameras, while not great for stereoscopic analysis, ended up being on plane with each breast, limiting depth parallax error during the jumping studies.

Figure 25. GoPro Camera, Blacklights, and Treadmill Setup



All participants had pasties (with fluorescent markers) covering their areola regions. All participants also had ECG-electrode-double-sided tape with fluorescent markers covering the remaining breast tissue, torso, and sternal markers. For the first subject, all markers were made with fluorescent paint applied to the pasties and ECG tape and allowed to dry before the subject arrived. While a stochastic distribution of paint using various brushes was successfully performed experimentally, it was deemed too invasive and time consuming to undertake for each subject. Instead, for subjects 2 through 4, fluorescent red vinyl was drag-knife-cut into 6mm circles and applied to the pasties and ECG tape. For subjects 5 through 7, fluorescent vinyl was drag-knife-cut into 10mm circles with 5mm holes cut into the centers. While this was done to facilitate tracking in GOM Correlate, the calibration again negated its full implementation until a better camera system and trigger can be acquired. Example raw footage from the GoPro can be seen in Figure 26, showing both the circles and circles with holes under blacklights only.

Figure 26. Raw GoPro 120 FPS Video, 530nm High-pass Filtered under Blacklights (*Upper: fluorescent 6mm dragknife-cut vinyl-film markers, Lower: 10mm circles with 5mm holes dragknife-cut vinyl-film markers*)



Durometer Quantification and Comparison

All participants had their breast firmness evaluated using the same FO-type durometer and location grid as was used for the first version of the simulator. To aid in display of this data, the grid pattern was numbered as shown in Figure 27. This numbering scheme was the same for both the right and left breasts meaning that, for instance, the medial aspect of the left breast would encompass grid locations 1, 4, and 7, while the same medial aspect of the right breast would encompass grid locations 3, 6, and 9. While not entirely optimal, this numbering scheme was maintained through data collection and presentation for consistency.

Figure 27. Durometer Grid Location Numbering

1	2	3
4	5	6
7	8	9

Demographic data was collected for each subject as shown in Table 6. This includes the miles per hour (MPH) at the metronome stride rate of 150 beats per minute (BPM). From this MPH and BPM, the stride length for each participant was calculated. The variation in torso and chest measurements versus the self-reported bra size illustrates that measurements do not always correspond with self-selected bra size. No subjects had previously had children.

Table 7 shows the durometer values of subject numbers 1 through 7 for both the left and right breasts. These durometer values and standard deviations per location closely mimic the range of values and variations seen, per location, of simulator version 1 at the 1:1 ratio. Per location the FO-type durometer has a standard deviations up to 4. The simulator has a per location standard deviation of approximately 2. The standard deviation over the entirety of the grid locations is much greater. The durometer readings vary around the breast locations with the

areolas region generally being the least firm location as expected since under the areolas the breast tissue is generally thickest. Of interest is that the durometer readings are slightly firmer (higher number) on the right breast versus the left breast. This may be because right-handedness is more prevalent among the general population (although handedness was not recorded during this study). Overall, these values confirm the simulator firmness range as being within the range of the subjects evaluated in this study.

TABLE VI. DEMOGRAPHIC CLINICAL SUBJECT DATA

	MPH @ 150 BPM	Stride Length (cm)	Torso (cm)	Chest (cm)	Age Group (Years Old)	Self-Report Bra Size
Subject #1	4.1	73.3	87	96	28-36	32D
Subject #2	3.9	69.7	73	82	37-45	34B
Subject #3	4.7	84	73	85	18-27	32D
Subject #4	4.1	73.3	80	90	37-45	34B
Subject #5	4.8	85.8	75	90	18-27	34C
Subject #6	3.6	64.4	67	84	18-27	32B
Subject #7	5.0	89.4	67	84	18-27	34B

While this study was not designed to correlate firmness with demographic information, these values show that simulator version 1 (formulation 1) is an acceptable mimic of anthropometric firmness values. This confirms that this formulation is a viable substitute for human bra-fit models regarding firmness of the breast tissue. While this study does not evaluate torso tissue firmness or more three-dimensional evaluation of breast tissue, it does provide evidence that, within the subject population evaluated, the range of firmness falls within the range of the simulator.

The least firm subject is number 5, an 18-27-year-old woman with a self-selected bra size of 32C. The firmest subject is number 4 who is a 37-45-year-old woman with a self-selected bra size of 34B. All remaining subjects are distributed within these two extremes, with the precision

of the durometer technique not generally being able to discriminate differences between subjects’ firmness.

TABLE VII. DUROMETER CLINICAL SUBJECT DATA

	LEFT BREAST									
	1	2	3	4	5	6	7	8	9	TOTALS
Mean Subject #1	29.0	28.0	20.0	27.3	25.7	29.3	22.7	24.3	17.7	24.9
Standard Deviation	0.0	3.5	0.0	3.8	2.5	0.6	2.1	2.5	1.2	6.7
Mean Subject #2	21.0	15.0	23.3	17.0	11.7	20.7	16.3	12.0	18.3	17.3
Standard Deviation	4.6	3.5	0.6	0.0	1.5	1.5	2.5	1.7	0.6	6.9
Mean Subject #3	20.0	20.0	14.7	19.7	25.0	24.3	25.3	25.3	17.0	21.3
Standard Deviation	0.0	0.0	0.6	1.5	1.7	2.3	1.5	0.6	2.6	4.5
Mean Subject #4	36.7	26.7	35.0	29.0	17.0	41.0	25.3	23.0	24.3	28.7
Standard Deviation	1.5	2.1	2.0	1.0	0.0	1.7	3.5	0.0	1.5	5.4
Mean Subject #5	12.7	14.0	13.7	9.7	1.7	6.3	10.7	6.7	7.0	9.1
Standard Deviation	2.5	1.7	3.5	1.5	0.6	1.2	0.6	0.6	1.0	5.2
Mean Subject #6	27.3	30.0	21.0	22.7	13.0	16.3	16.7	21.0	17.3	20.6
Standard Deviation	2.1	2.0	2.6	1.5	1.7	1.5	1.5	1.7	2.5	5.9
Mean Subject #7	26.3	20.7	24.0	15.0	13.0	32.7	23.7	24.7	28.0	23.1
Standard Deviation	2.3	1.2	1.7	1.0	0.0	2.1	3.5	1.5	2.0	5.8
Location Mean	24.7	22.0	21.7	20.0	15.3	24.4	20.1	19.6	18.5	20.7
Standard Deviation	6.3	6.1	5.2	4.8	3.9	4.4	6.4	3.9	4.7	15.4

	RIGHT BREAST									
	1	2	3	4	5	6	7	8	9	LEFT TOTAL
Mean Subject #1	24.3	24.3	26.0	22.0	21.3	23.3	18.7	22.3	21.0	22.6
Standard Deviation	1.2	0.6	2.6	1.0	1.5	2.1	1.5	0.6	1.0	4.5
Mean Subject #2	24.3	19.0	19.7	26.3	11.7	15.7	23.0	12.7	17.3	18.9
Standard Deviation	1.5	2.0	1.2	1.2	2.1	1.5	4.0	1.5	0.6	5.9
Mean Subject #3	25.7	30.0	23.3	23.0	20.7	25.0	25.7	19.7	26.3	24.4
Standard Deviation	1.2	3.0	2.1	1.0	2.3	1.0	0.6	0.6	2.3	5.3
Mean Subject #4	37.3	21.7	26.3	32.7	20.0	26.7	33.7	26.3	21.7	27.4
Standard Deviation	0.6	0.6	0.6	2.3	1.7	0.6	1.5	0.6	0.6	3.6
Mean Subject #5	10.0	16.0	12.7	11.0	2.3	11.0	8.7	5.7	6.0	9.3
Standard Deviation	1.0	0.0	2.5	1.0	0.6	1.7	2.1	2.5	1.0	4.8
Mean Subject #6	22.0	23.7	36.7	22.3	16.0	30.0	21.0	25.0	30.3	25.2
Standard Deviation	0.0	1.2	1.5	2.1	1.0	2.0	1.0	1.0	0.6	3.9
Mean Subject #7	14.0	20.3	23.3	20.3	10.7	25.0	27.3	21.7	25.3	20.9
Standard Deviation	1.0	1.2	1.2	1.2	1.2	1.0	2.1	0.6	2.1	4.0
Location Mean	22.5	22.1	24.0	22.5	14.7	22.4	22.6	19.0	21.1	21.2
Standard Deviation	2.7	4.0	4.8	3.9	4.2	4.0	5.5	3.3	3.6	12.2

Dynamic Quantification and Comparison

From the complete datasets of the clinical study, only select examples were chosen for discussion and comparison here. These presented datasets are representative of each subject and generally there was similarity within an individual between, for instance, the first jumping dataset and other jumping datasets. Mostly running, either in place or while the treadmill was moving, is ignored as the motion is more complex and confounding compared to jumping which

more closely mimics simple vertical motion. The lack of 3D depth in the motion capture analysis is accepted as a limitation of the on-plane single camera system utilized.

Figure 28 shows subject 1's right breast during jumping and displays how the jumping motion transpired with most subjects. The initial downward motion of the torso caused the areola to initially move upward until the torso began to move upward again. This abrupt change to positive acceleration caused the areola to overshoot its initial position relative to the torso and sag in response to the upward acceleration. The upward acceleration of the torso slowed under gravity, as well as the sagging of the breast areola, followed by the overshoot of the areolas after deceleration of the torso crossed zero, and the torso began accelerating downward. Upon foot landing, the torso moved rigidly back to its initial position while there was a small oscillation of the torso and subsequent oscillation of the relative areola position.

Subject 1 shows comparatively rigid jumping and landing with minimal oscillation of the torso upon landing. This oscillation of the torso upon landing may be in part because the treadmill was not rigid or because of muscle force control being underdamped instead of being critically damped, or some combination of the two. Another possibility is this subject's muscle control is minimizing breast movement by compensating for areolas motion. Although the underlying cause of this torso oscillation may confound reproduction of rigid vertical motion it, may mimic the force-based control and oscillation of the pneumatic version 1 simulator.

Subject 1 shows minimal horizontal motion of the areolas or the torso, showing mostly vertical motion overall. The slight horizontal motion that does exist is shown in the traces of the vertical and horizontal motion together, showing a slight medial motion of the areola at the extremes of its motion relative to the torso. The traces of the horizontal and vertical accelerations respectively and combined show how the vertical accelerations are far greater than the horizontal

accelerations. The acceleration of the areola vertically was greatest while the torso was falling, and the greatest deceleration occurred upon landing. The horizontal acceleration and deceleration extremes were less consistent in this subject but follow the timing of falling and landing respectively.

Figure 29 shows Subject 2's right breast and looks very much like subject 1, with greater oscillation intensity after landing. The accelerations and displacements are also greater than subject 1. The dual horizontal and vertical accelerations show more characteristic circular motion during positive acceleration excursions of the areola.

Figure 30 shows Subject 3's left breast and looks very much like subject 2's right breast but accelerates medially in the other direction as shown in the dual horizontal and medial displacement traces. Circular traces are evident in the dual acceleration graph. A limitation of the single camera is shown by the diverging traces at the end of recording caused by parallax error from a slight depth change. These offsets may be noticed and are accepted to impact data quality.

Figure 31 shows Subject 3's left breast during running. Notice the shorter time on the x axis of the graphs and the increased intensity of the accelerations and displacements. Notice the large areola accelerations but short vertical travel. The areola accelerations during running are greater than jumping in this subject. Also shown is the figure-eight-shaped displacement traces and circular-motion acceleration traces.

Figure 32 shows Subject 4's large accelerations of the right areola at landing and the large oscillations of the areola after this landing. This subject shows similar displacement traces as other right areolas, such as those shown in Subjects 1 and 2. Also similar is the circular motion on the dual horizontal and vertical acceleration traces.

Figure 33 shows an increasing acceleration as Subject 5 exerts more effort jumping. The vertical motion profile shows how the subject bends down more to jump higher. There is a high degree of oscillation. Also, there is very little horizontal acceleration. Otherwise, this subject shows a typical right areola.

Figure 34 shows Subject 6 with the least displacements. The greatest vertical accelerations occur upon landing. The acceleration traces are very minimal in horizontal and vertical travel.

Figures 35 and 36 are both datasets of Subject 7 and illustrate the similarity of motion profiles between replicants. The left breast has motion displacement traces showing the areola being thrown laterally and upwardly in a circular manner. The oscillations in this subject are minimal, but the landing-impact areola accelerations remain the same.

Figure 28. Subject 1 Jumping Right Breast (Top Left: Vertical Motion in meters, Top Right: Horizontal Motion in meters, Bottom Left: Vertical Acceleration in meters/second², Bottom Right: Horizontal Acceleration in meters/second²; Blue: torso, Orange: areola + torso, Grey: relative areola)

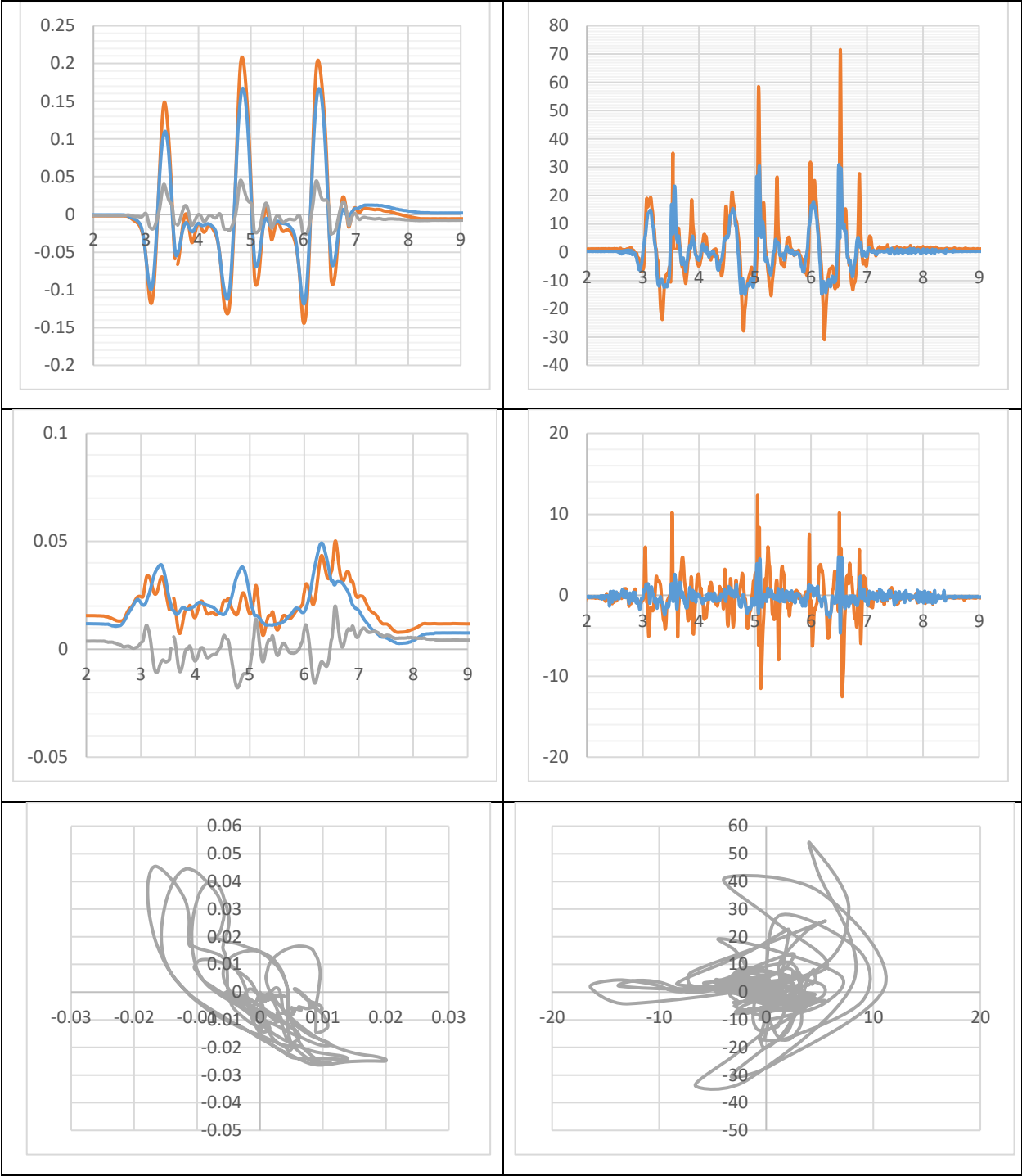


Figure 29. Subject 2(4) Jumping Right Breast (Top Left: Vertical Motion in meters, Top Right: Horizontal Motion in meters, Bottom Left: Vertical Acceleration in meters/second², Bottom Right: Horizontal Acceleration in meters/second²; Blue: torso, Orange: areolas + torso, Grey: relative areolas)

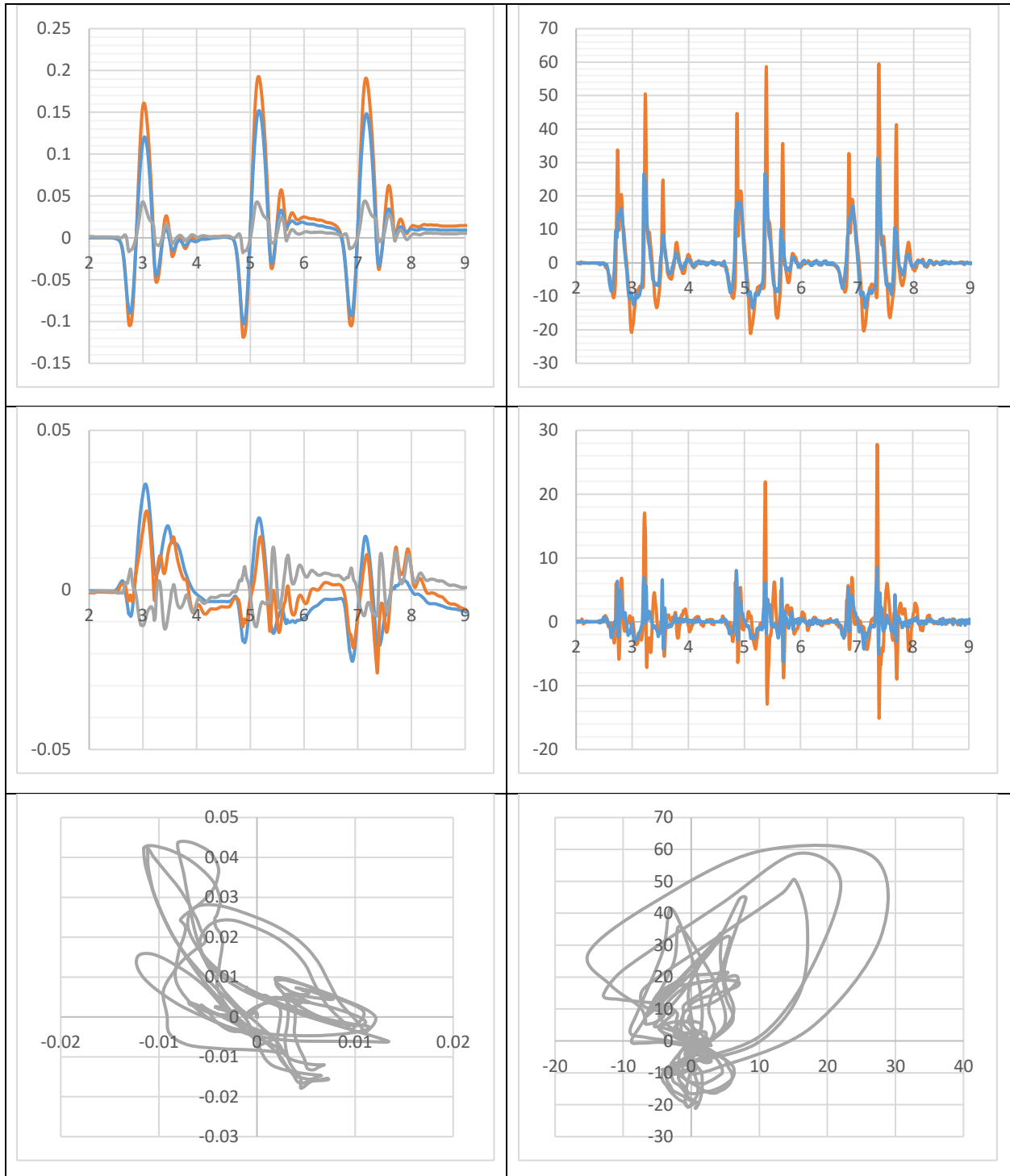


Figure 30. Subject 3(2) Jumping Left Breast (Top Left: Vertical Motion in meters, Top Right: Horizontal Motion in meters, Bottom Left: Vertical Acceleration in meters/second², Bottom Right: Horizontal Acceleration in meters/second²; Blue: torso, Orange: areolas + torso, Grey: relative areolas)

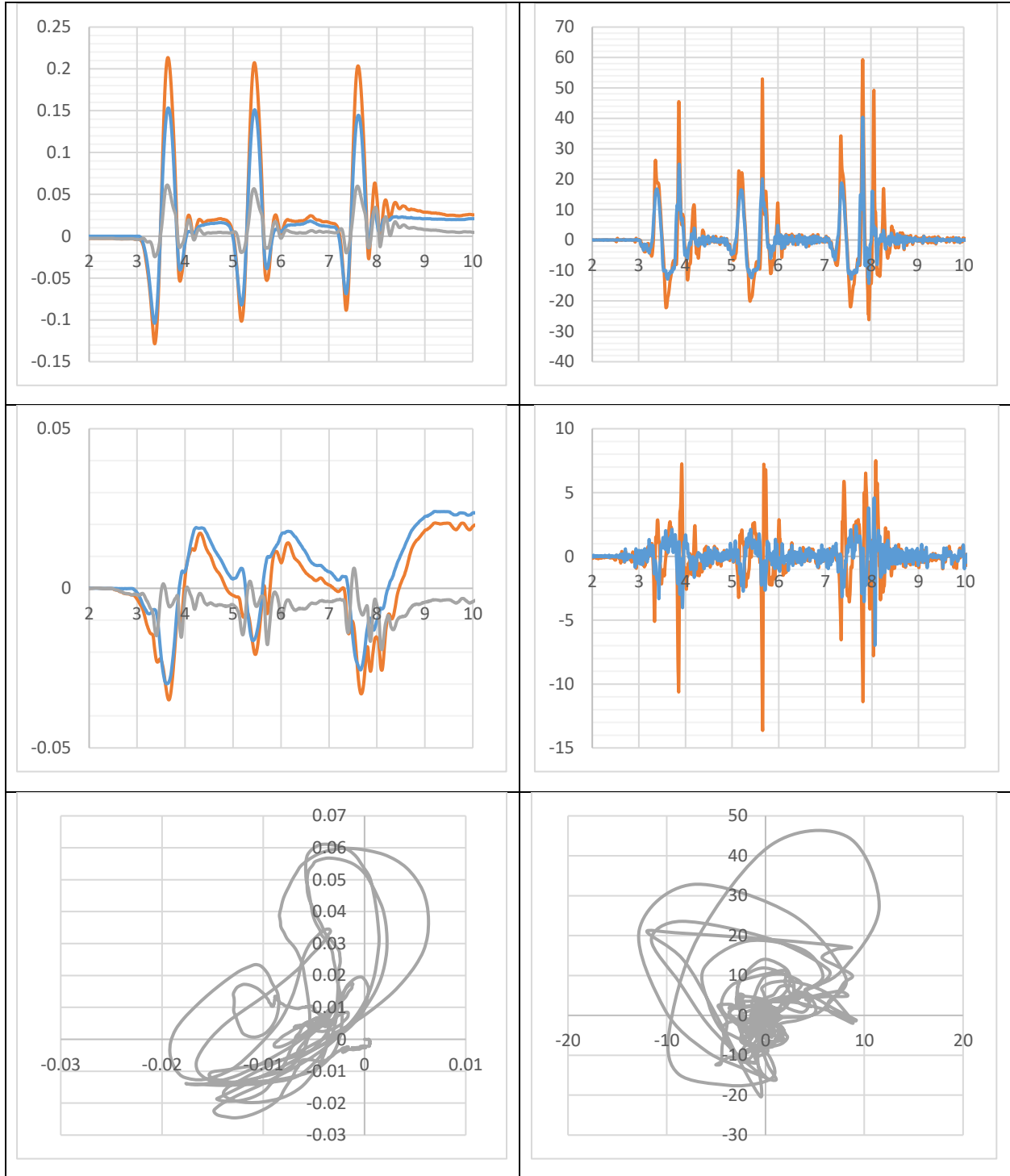


Figure 31. Subject 3(6) Running Left Breast (Top Left: Vertical Motion in meters, Top Right: Horizontal Motion in meters, Bottom Left: Vertical Acceleration in meters/second², Bottom Right: Horizontal Acceleration in meters/second²; Blue: torso, Orange: areolas + torso, Grey: relative areolas)

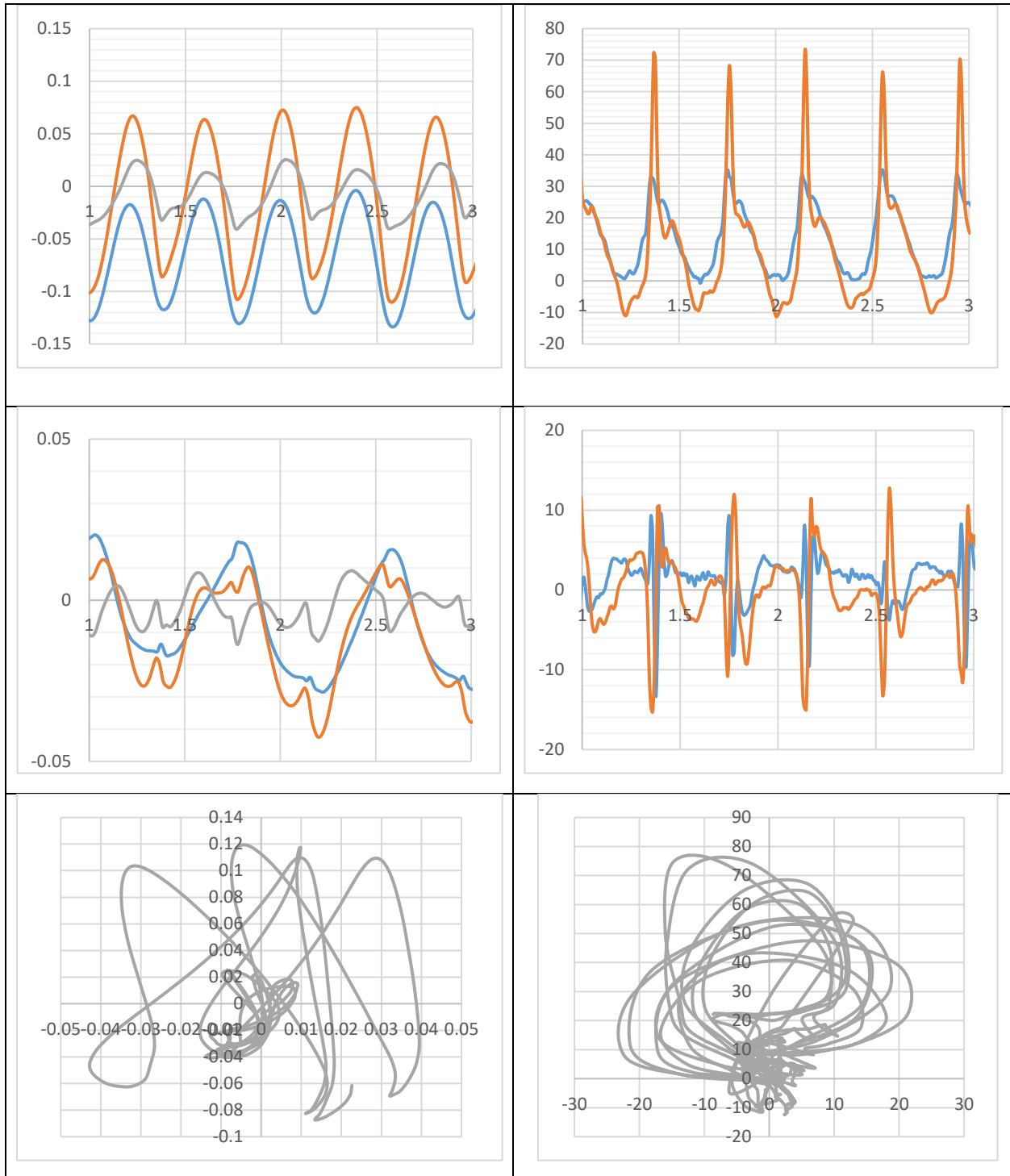


Figure 32. Subject 4(7) Jumping Right Breast (Top Left: Vertical Motion in meters, Top Right: Horizontal Motion in meters, Bottom Left: Vertical Acceleration in meters/second², Bottom Right: Horizontal Acceleration in meters/second²; Blue: torso, Orange: areolas + torso, Grey: relative areolas)

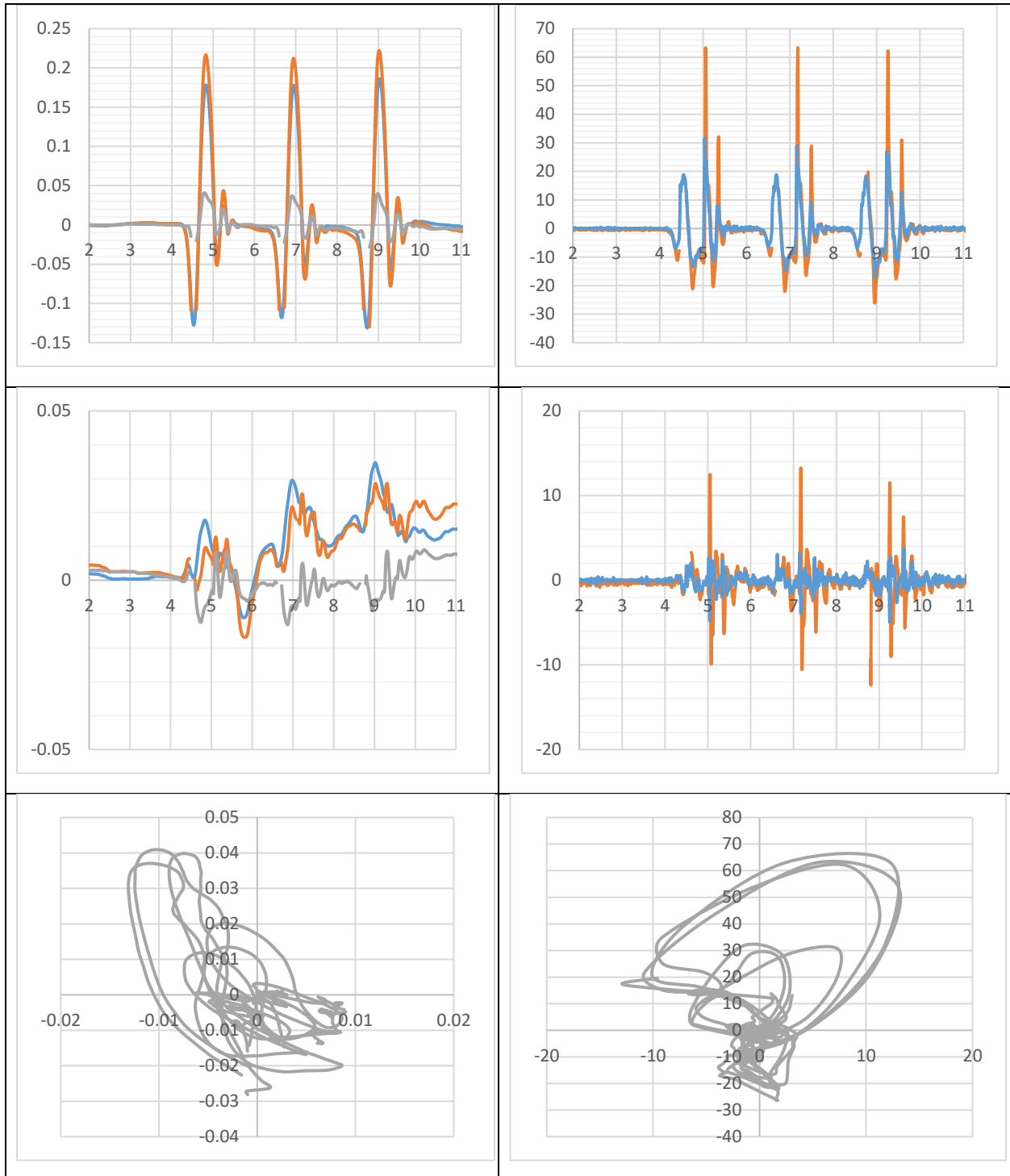


Figure 33. Subject 5(7) Jumping Right Breast (*X Axis: seconds; Top Left: Vertical Motion in meters, Top Right: Horizontal Motion in meters, Bottom Left: Vertical Acceleration in meters/second², Bottom Right: Horizontal Acceleration in meters/second²; Blue: torso, Orange: areolas + torso, Grey: relative areolas*)

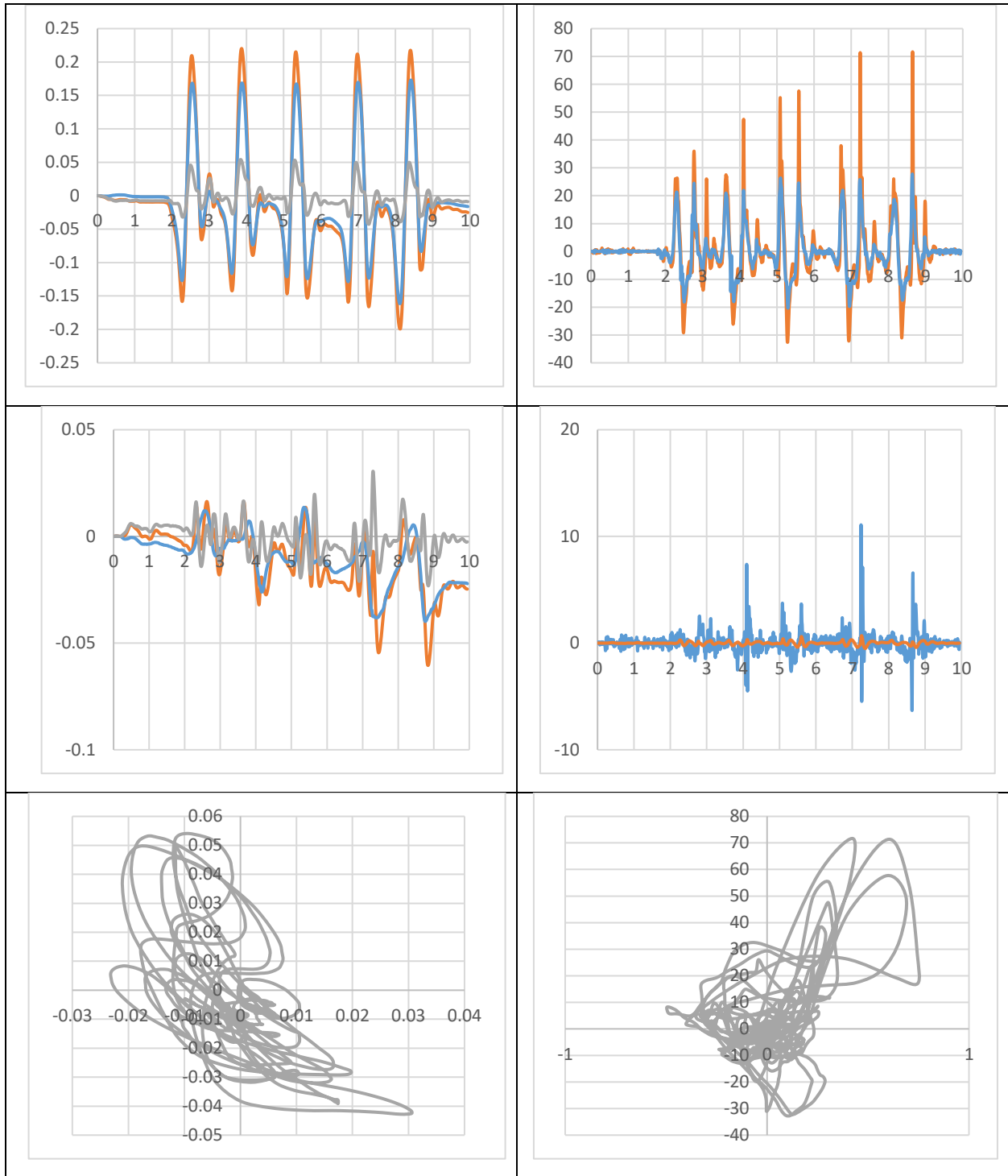


Figure 34. Subject 6(4) Jumping Right Breast (Top Left: Vertical Motion in meters, Top Right: Horizontal Motion in meters, Bottom Left: Vertical Acceleration in meters/second², Bottom Right: Horizontal Acceleration in meters/second²; Blue: torso, Orange: areolas + torso, Grey: relative areolas)

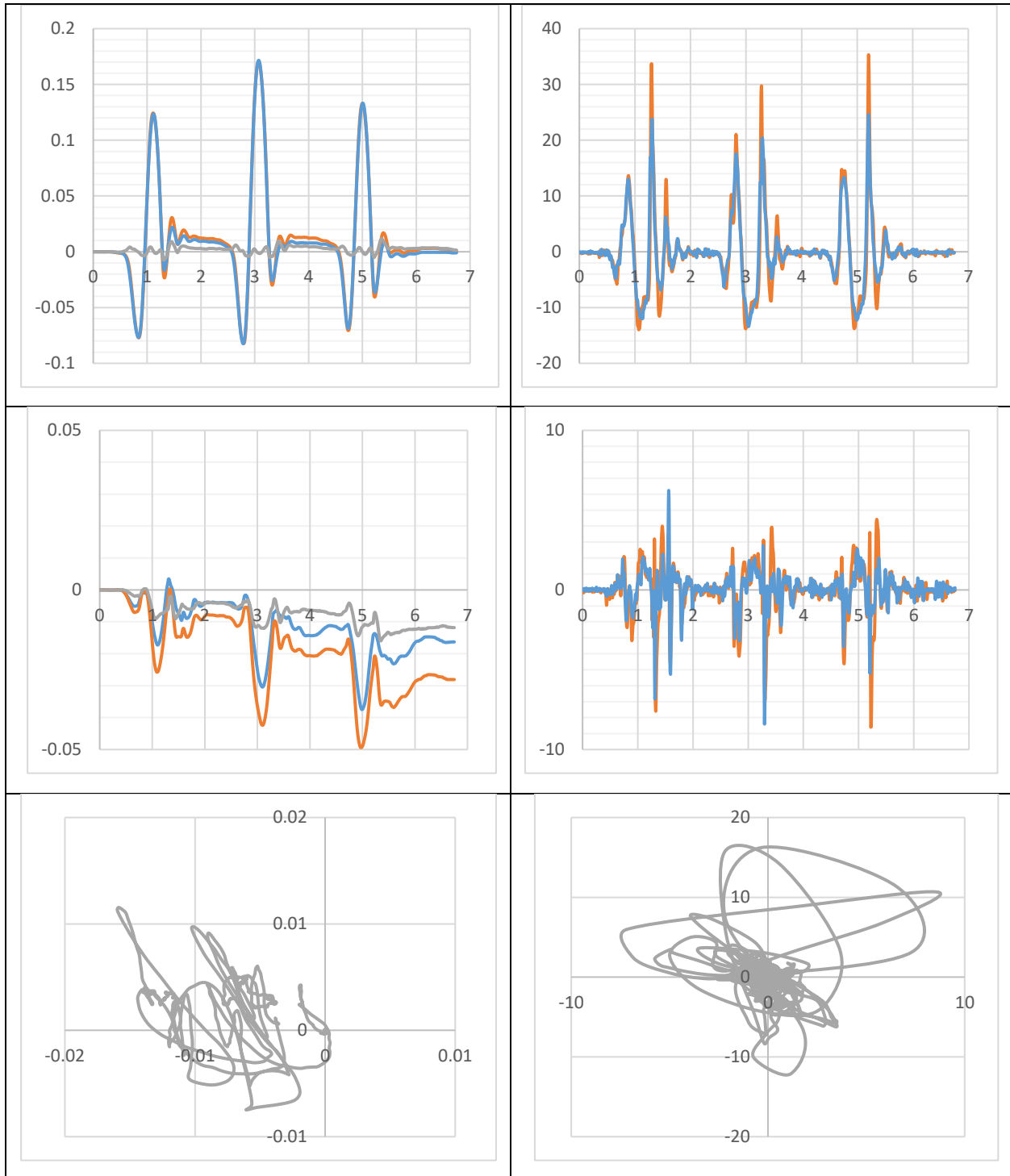


Figure 35. Subject 7(387) Jumping Left Breast (X Axis: seconds; Top Left: Vertical Motion in meters, Top Right: Horizontal Motion in meters, Bottom Left: Vertical Acceleration in meters/second², Bottom Right: Horizontal Acceleration in meters/second²; Blue: torso, Orange: areolas + torso, Grey: relative areolas)

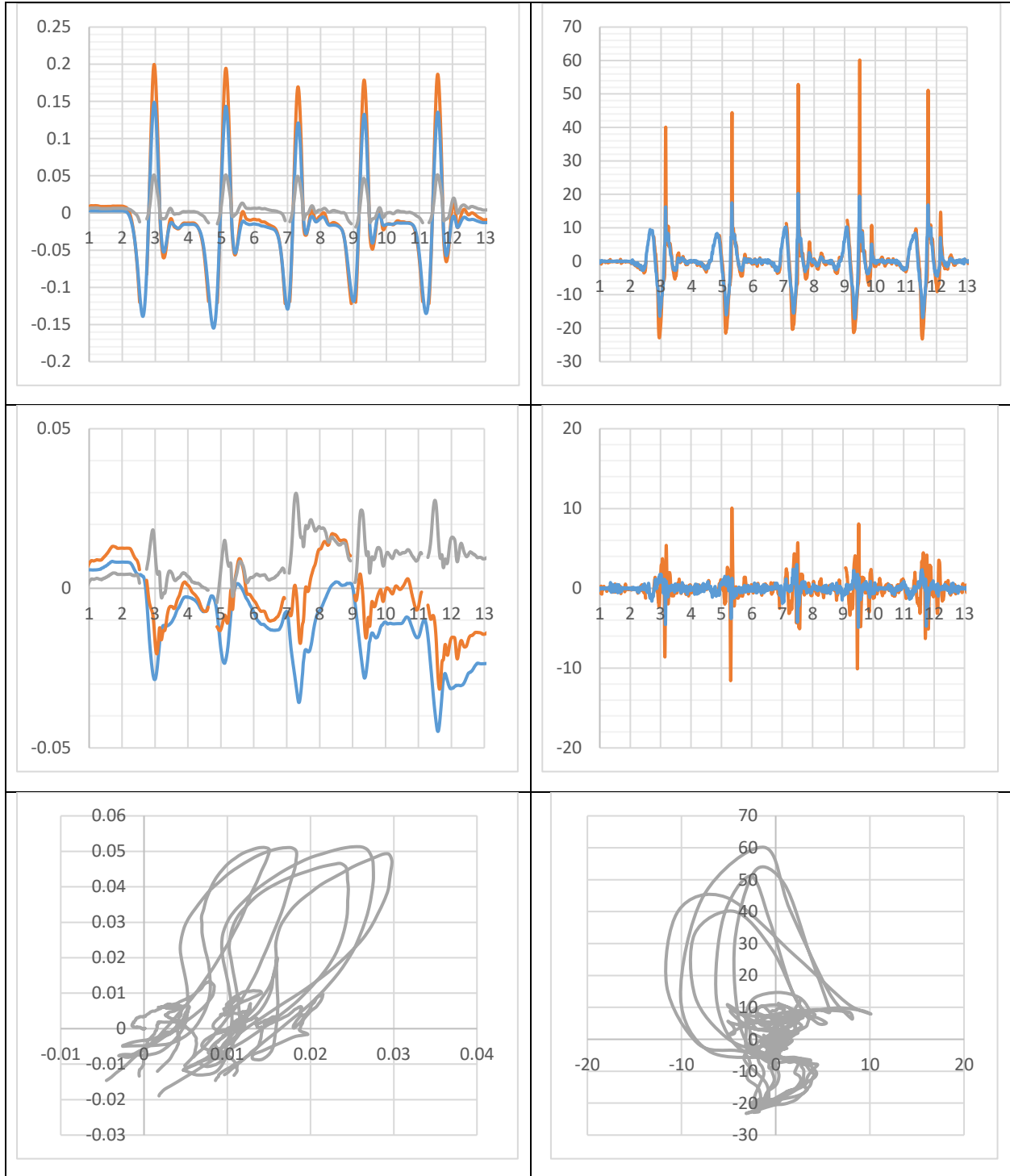
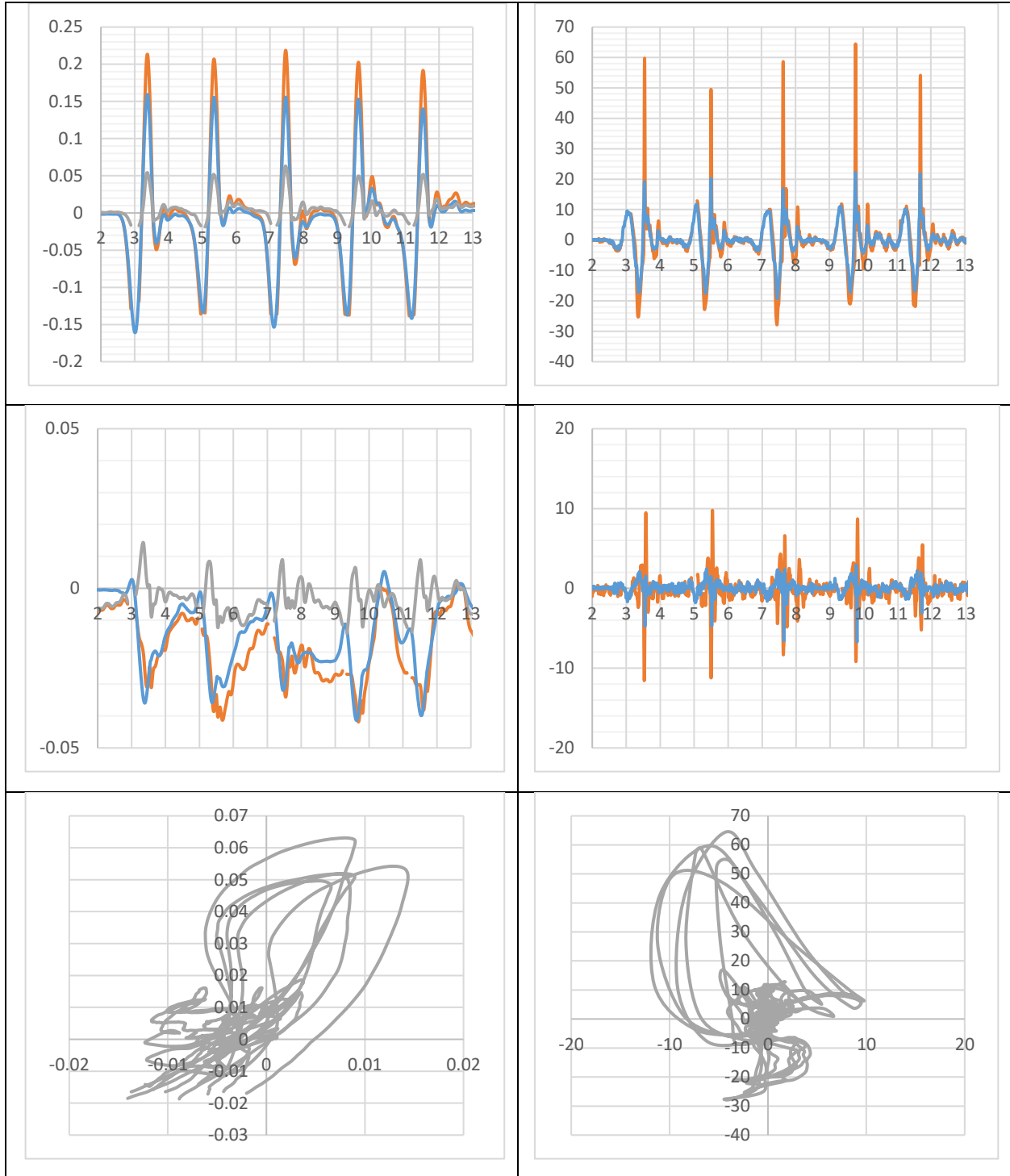


Figure 36. Subject 7(389) Jumping Left Breast (X Axis: seconds; Top Left: Vertical Motion in meters, Top Right: Horizontal Motion in meters, Bottom Left: Vertical Acceleration in meters/second², Bottom Right: Horizontal Acceleration in meters/second²; Blue: torso, Orange: areolas + torso, Grey: relative areolas)



CHAPTER 5: FEMALE BREAST, TORSO, AND MOTION SIMULATOR 2

Version 1 of the simulator provided evidence that a robotic breast motion simulator could be used to evaluate breast firmness and dynamics. This first version demonstrated anthropometric firmness simulation, although the simplified molding and lattice structure were not thoughtfully designed and engineered. The first pneumatic vertical motion stage proved lackluster for simple motion modeling and point-by-point positional control. This force-based aspect of motion may be like aspects of human muscle unit recruitment and control motion profiles. Despite these positive attributes of simulator version 1, there exists a need to provide a rigidly coupled hybrid servo vertical motion stage.

After evaluation by vested parties, end users, and self-review, the simulator torso was decidedly not well designed: not the molding process nor the original 3D file reproduction, not the skin thickness nor the lattice structure, not the rotational servo nor the torso mount, not the housing and accessibility to the torso for fitting, and not the overall simplicity of the dynamic and static fit analysis. For these and other reasons, improvements to the design of the simulator were undertaken with the intent to provide a turn-key solution to the end user for bra-fit testing as well as a cheaper and easier simulator to manufacture and transport. These changes and new custom sensor integrations necessitated the design of a new, version 2 of the breast motion simulator.

Design Reasoning and Method of Build

In the second torso version, the 3D printed nylon lattice was thickened to 3mm to impart greater strength. As shown in Figure 38, the lattice structure was built directly from the surface

edges at 8mm uniformization while other sizes were explored. The skin in this new version was thickened to 6mm, requiring an offset in the processed scan surface to create the now offset lattice. Since the lattice thickened bilaterally 1.5mm (3mm total thickness), the digital surface of the processed scan was internally offset 7.5mm to produce a 6mm offset nylon surface. 30mm-wide sections at the top of the neck, the spinal column, and the bottom of the torso were solidified. These sections were Boolean added with the lattice as solid sections of 3mm thick nylon for reinforcement. The mount plate was maintained at 8mm thickness with a simple interface with the 3mm thick lattice without any ridge or other type of supports between the mount plate and the lattice. The final torso lattice and a comparison to version 1 of the lattice torso are shown in Figure 39.

In the second version of the torso, rather than using 3D printed molds, the processed scans were digitally shelled at 3mm inward thickness, and a full torso version with breasts and another version without breasts were 3D printed in SLS nylon as shown in Figure 37. These prints were sealed and waxed and then used as positives for making negative molds with Plasti-paste support shells. This technique proved to be a poor molding solution, and thus the development of 3D printed negative molds was undertaken.

For the 3D printed negative molds, the torso sans breasts or torso with breasts was thickened outwardly 3mm. This shell was sectioned into four pieces, and two 8mm-thick sections were added to both sides of each shell section. While these sections were 8mm thick, they represented a 30mm outward offset of the original scan with the original scan Boolean subtracted from them. These 8mm (30mm offset) sections provided interface and connection between the sections of this shell-based mold. When the mold sections were aligned and the 8mm thick interfaces were held together with 2.5-inch binder clips, they created a full-torso-

sans-breast or torso-with-breasts mold. As shown in Figure 40, these molds provided an offset of 6mm thick for silicone-simulated skin, but the torso had to be aligned within the mold cavity.

As shown in Figure 43, the silicone tubing (5mm outer diameter, 3mm internal diameter, Shore A35) was wrapped around the torso, as a dual use solution, both as a spacer around the torso to center it within the mold and as a sensor to measure the pressure within the silicone skin layer. This centering of the lattice torso within the mold provided the best silicone skin thickness uniformity. The 5mm tubing also provided for sensing the silicone skin pressure, but to prevent collapse during molding, the tubing was capped with a hose barb plug.

The lattice itself was modified to accommodate the entrance of the silicone tubing into the lattice to allow the attachment of hose barb connectors and sensor attachments. Figure 43 shows where holes were sculpted into the spinal-column-solid-nylon-reinforced section to allow entrance of the tubing. Figure 42 is a visual approximation of how the spinal column fits within the torso and the approximate intervertebral space positioning. The spacing of those holes was chosen to be more anthropometric according to the distances calculated from human intervertebral spaces C7-T1 through L1-L2 and located according to palpation of the torso's C7 spinous process.³⁷

Ten circumferential tubing sensors enter the lattice at intervertebral spaces T4-T5 through L1-L2 while the pairs of tubing sensors over the upper shoulder enter the lattice at C7-T1 and T1-T2 intervertebral spaces. The lower pair of shoulder tubing sensors exits at T2-T3 and T3-T4. As shown in Figure 44 within the lattice torso, each silicone tube was attached to itself through T-connectors which then each attached to a 7/32-inch ID 3/32-inch ID polyethylene tube. The polyethylene tubes were routed either to the inner rim of neck, as shown in Figure 44, or routed to the inner rim of the bottom of the torso (not shown) and finally sutured in place to the inner

surface of the lattice. Before introduction into the mold, each polyethylene tube was plugged shut with a hose barb plug to prevent the tubing from collapsing.

The molding process for simulator version 2 can be undertaken similarly to simulator version 1 by using FEP sheets, making a skin layer on the inner surface of the torso with breasts mold, and backfilling with silicone gel. This process, however, is difficult to obtain, and thus various tubing sensor configurations and constructions within the skin layer and breast tissue are currently being explored. Before introduction of the silicone tubing and lattice into the mold, they are washed with isopropanol to promote adhesion and are made watertight with one or two applications of 00-10 Ecoflex silicone that is allowed to drip off under surface tension as shown in Figure 43. The current molding process then starts by placing the watertight lattice torso with silicone tubing into the mold and filling it with 00-10 Ecoflex silicone which may have a ratio of 1:1 or up to 1.2:1, producing a softer and more flexible silicone skin layer.

The molding of the torso sans breasts is undertaken in sections starting with sealing any remaining non-watertight regions of the holes cut into the spinal column area by placing the filled mold towards at an angle where the mass of the silicone flows onto the back. The mold and torso are positioned so silicone flows, under gravity, toward the neck and over the back while the area between the lattice neck and the mold is sealed with silicone strips or paper towels to prevent silicone running out through the top of the mold. Any holes or bubbles that may develop during molding can be removed and any sections not solidly filled can be filled with silicone and remolded in the torso-sans-breasts mold until the skin is solid and uniform over the surface.

Only after molding of the torso sans breasts is complete is the mold lattice torso plus skin and tubing placed into the mold for the torso with breasts. As a more durable alternative to creating a separate breast silicone skin and breast tissue silicone gel composite, a uniform

silicone alone may be used for the breast skin and tissue without any silicone gel. To make the breasts less firm and to integrate breast-only-pressure-sensor tubing, integration of a mass of tubing into the silicone-only-breast skin and tissue is being explored.

After the final torso with breasts is molded onto the lattice with silicone, all polyethylene tubing is unplugged and attached to a T-connector. This T-connector is itself connected to both a luer-lock needle-free injection port valve for pressure equilibration and a board mounted MPXV7002 sensor for quantification of the pressure reading through the silicone tubing sensors. The range of measurements is between positive and negative 2.5 kilopascals, but before use each sensor requires offset removal and equilibration with the surrounding air pressure since the MPXV7002 is a dual port relative pressure sensor. Initial testing of this pressure sensing tubing shows significant pressure changes upon application of a test bra to the simulator prompting further development and design of the sensing tubing and placement. This range of pressure measurement is relevant to bra fit quantification as anywhere from tens to multiple hundreds of pascal pressure change occur with bra fit.

The pressure sensor analog outputs are analog multiplexed with a 16 channel CD74HC4067 analog multiplexer into the 3.3v analog input of a HELTEC ESP8266. The ESP32 is currently being used instead as it has a more forgiving input voltage range compared to the 3.3v of the ESP8266 which requires using the ratiometric MPXV sensors at 3.3v which is outside the datasheet quoted range of the sensor. The point of using either microcontroller is to provide wireless data transfer and ease use of the sensors array with the system, negating wire attachment between the final molded torso and the rest of the simulator. Each microcontroller was programmed in the Arduino programming environment using manufacturer-provided compiler abstraction. The microcontroller reading the sensor array communicates via UDP (with

auto network reconnect) to a Labview program on the host computer through a Wi-Fi router network. The OLED on the ESP8266 displays a graphical representation of the sensor outputs as well as connection IP addresses (not shown). While this Wi-Fi communication can ease attachment, the addition of the Wi-Fi router and the time syncing issues over Wi-Fi with the simulator may negate Wi-Fi in near term simulator improvements. The sensor array is currently being redesigned to enable an easy wired connection with the simulator to simplify sensor integration with other hardwired simulator motion information.

While the silicone tubing provides pressure sensing to give the end user a quantified feedback about garment fit and sizing, the tubing sensors are also being explored for use in dynamic evaluation of bra support and resistance to breast motion. To enable this dynamic motion and improve on the pitfalls of the previous simulator motion mechanics, a new rigidly coupled vertical stage was designed along with a more forceful rotational stage. As shown in Figures 46 and 47, this new simulator motion mechanics and housing provides vertical and rotational motion while easing access to the simulator.

For the vertical stage, a tensioned ANSI 35 hybrid metal/polymer chain is rigidly attached to the bottom of a 40mm x 80mm aluminum extrusion from OpenBuildPartStore.com and tensioned through a spring to the top of the extrusion. This setup provides greater than ten inches of vertical motion while providing minimum friction and only having modest non-linearity over its range-of-motion.

As shown in Figure 48, a 13-tooth sprocket is coupled to the shaft of a NEMA23 3-Newton-meter 3-phase DC servo (rotor inertia 0.7 gram-meter²) mounted to a plate attached to the main 12-wheel linear bearing plate assembly from Openbuildpartstore.com. This linear bearing plate is attached to the 40mm-by-120mm aluminum extrusion (500mm long) holding

together the upper and lower surfaces of the housing. This NEMA23 has subsequently been replaced with a NEMA34 hybrid servo (12-Newton-meter, 4 kilogram-centimeters²) powered directly from 110v.

As shown in Figure 49, atop the aluminum extrusion vertical axis, a HP MJF 3D printed nylon plate assembly attaches a NEMA23 2-Newton-meter 3-phase DC servo (rotor inertia 0.5 gram-meter²) to a 100mm hollow bearing through SLS nylon spacers. This motor is currently being replaced with the original vertical stage NEMA23 motor. Attached to the servo and bearing are four stainless steel 1.5-inch diameter magnets. These magnets, along with the rotational axis attached to the 80mm-by-40mm aluminum extrusion, slide flush into holes in the planar undersurface of the 3D-printed-nylon-lattice-torso mount plate.

On the inside of the torso lattice and on the inner surface of this mount plate, circular laser-cut 1/8-inch-thick magnetic tape with a 3/8-inch central hole is rolled and then inserted through the neck opening, carrying a central 3/8-inch nylon bolt, which is then threaded into the central mount plate hole using an extended hex socket head. The lower segments have a diameter of less than 3.5 inches, while the upper segments have a diameter of greater than 5.5 inches, allowing the magnets to slide into the mount plate holes and magnetically attach to the magnets. Originally, this magnetic tape was metal, but the attachment was much too strong. This magnetic tape provides easy and firm attachment of the torso to the simulator servo assembly.

The motion control of all axes' servo motor drivers is undertaken with a MyRIO board in which the splines are generated on the ARM processor in real-time as a pulse-generator and counter run on the FPGA. The same simple user interface for simulator 1 provides control of parameters: linear motion timing (pace) and range; start position offset; and rotational motion splines and phase offset. In the first simulator version, a square wave actuation of the

proportional valve produced an under-damped, sine-like motion path for the torso. As with the first, the second simulator allows control of range and phase-of-rotation of the torso. The importance of phase coordination at running versus walking speeds has been studied previously.³⁸ These aspects of breast motion may be explored further in the future.

As shown in Figures 46 and 57, the second simulator version housing consists of three casters, two 1-inch-thick, 22-inch diameter HDPE circular plates, and 500mm-long, 40mm-by-80mm aluminum extrusion sections arranged in three groups between the circular plates. A slot is milled into the circular plates for two overlapping, rotating polymer doors to slide through. A circular polypropylene sheet guard provides safety through sliding and locking bearings.

Figure 37. Uniformized Torso (left: with breast, right: sans breasts)

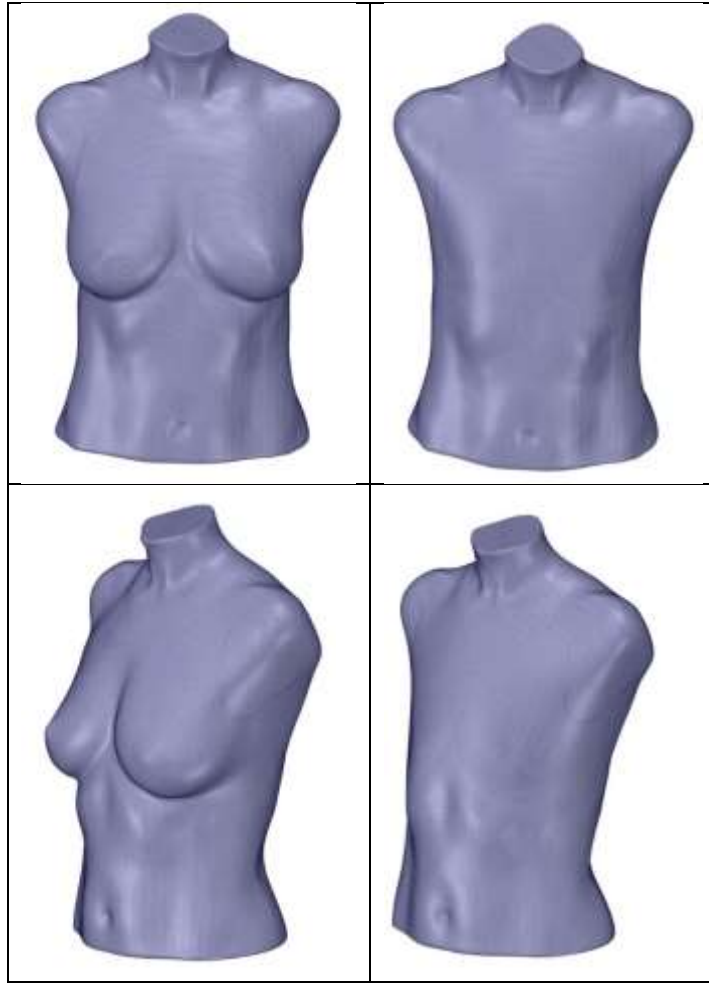


Figure 38. Uniformization Length Variations of Lattice (Version 2)

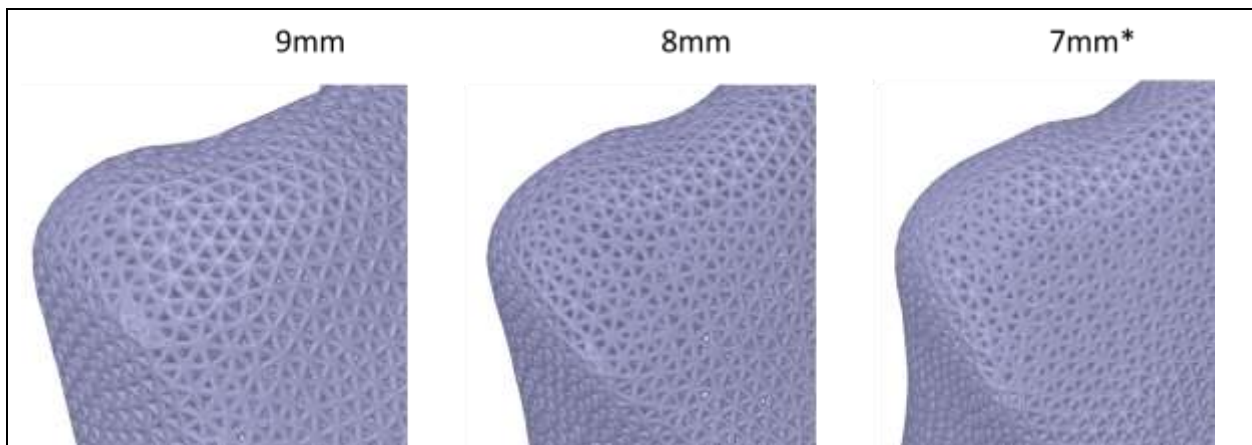


Figure 39. Simulator Lattice Version Comparison (*version 1 green, version 2 purple*)



Figure 40. Comparison of Lattices within 3D Scan (*Left: Version 1; Right: Version 2*)



Figure 41. SLS Nylon 3D Printed Mold around Torso (*Left: Sans Breast Torso; Right: with Breasts Torso*)

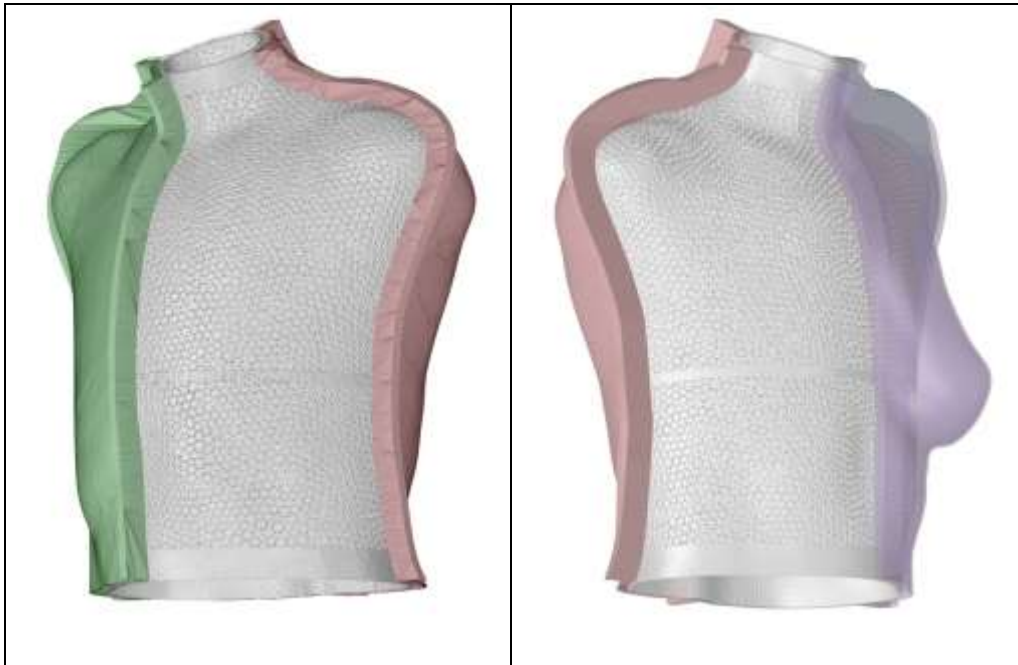


Figure 42. Representation of Spine within 3D Scan

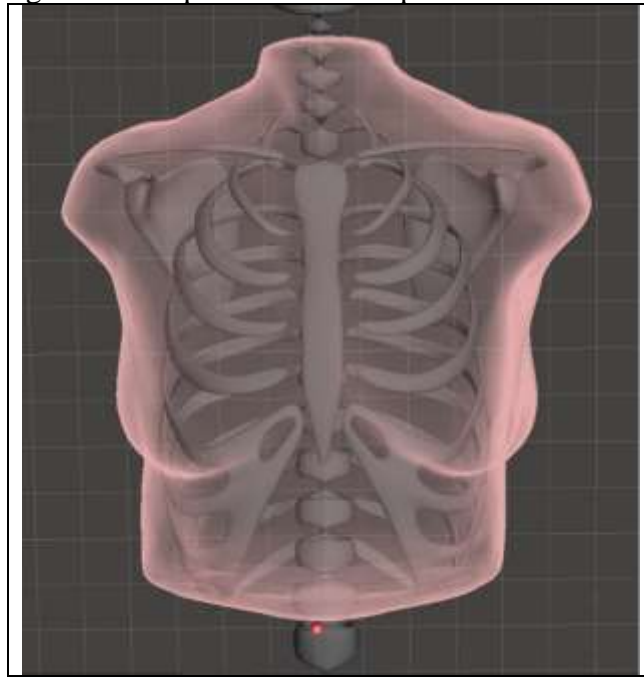


Figure 43. Pressure Sensor Tubing Placement (Version 2)



Figure 44. Simulator Tubing Management (Version 2)

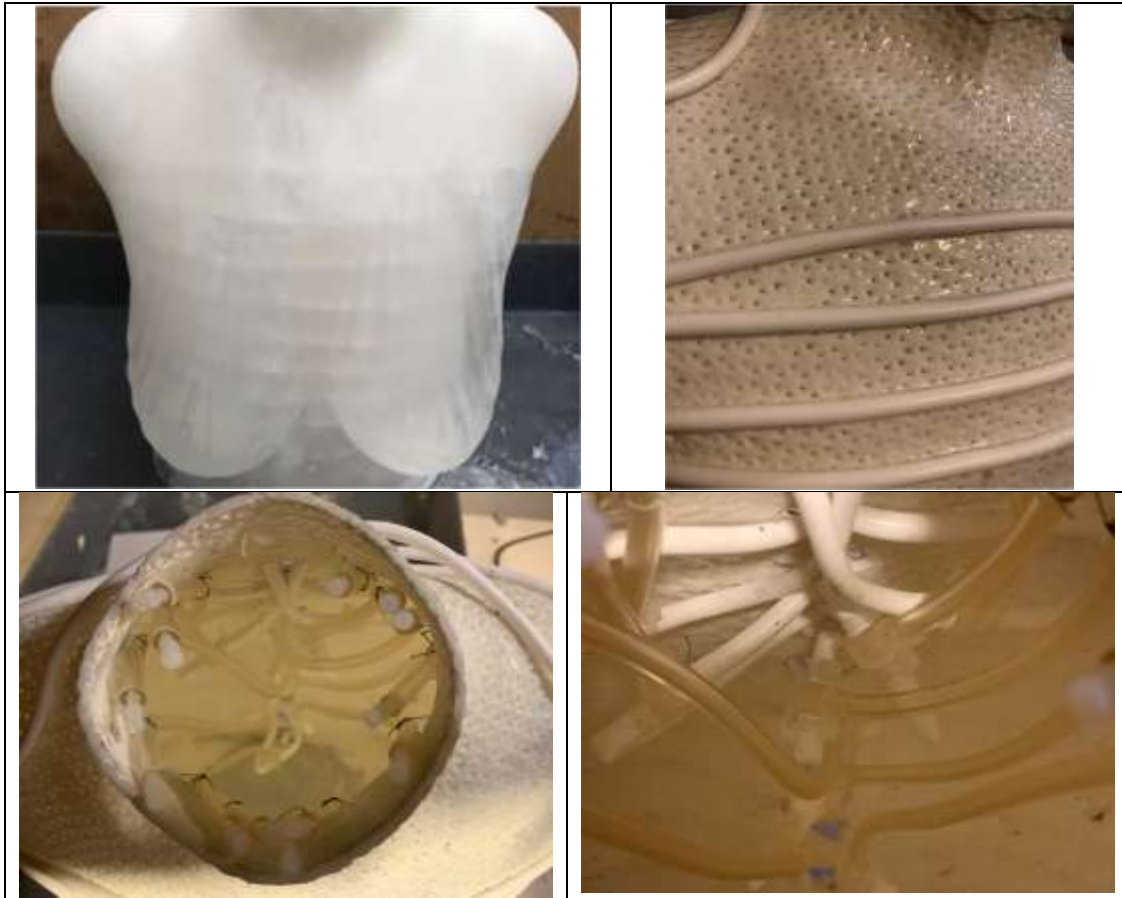


Figure 45. Breast Motion Simulator (Version 2)



Figure 46. Simulator Version 2 in Housing (from left to right shows vertical and rotational motion)

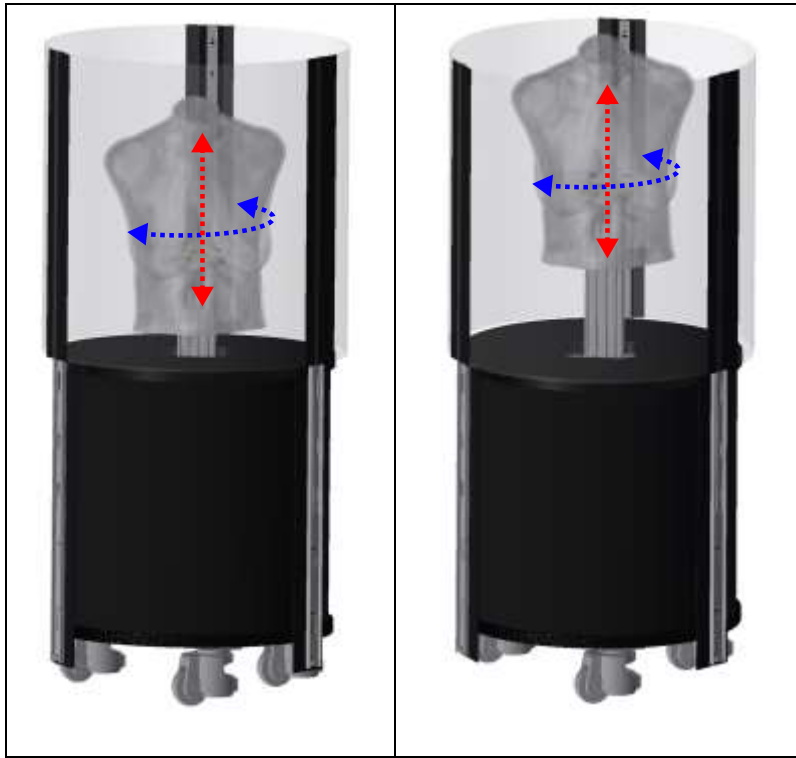


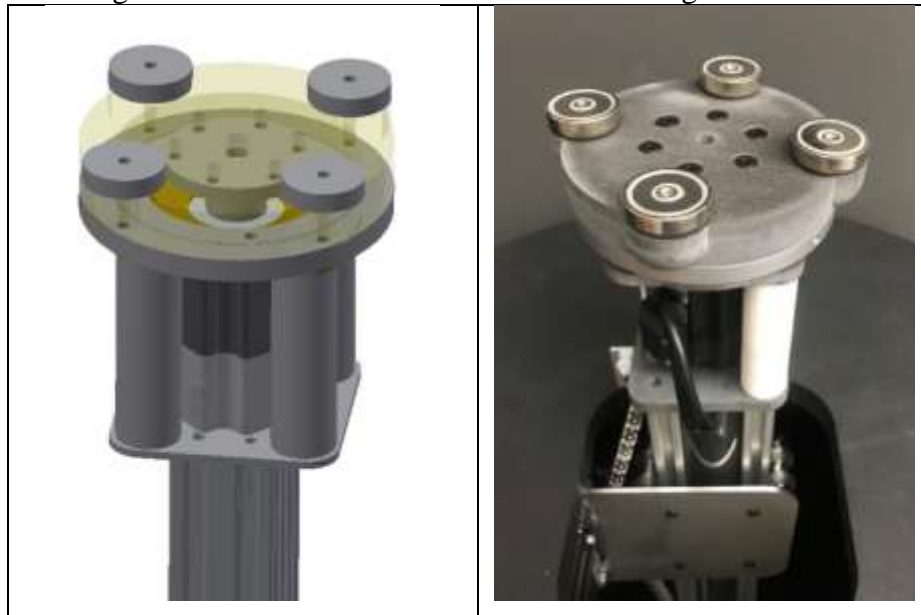
Figure 47. Servo Chain-Coupled Simulator in Housing (Version 2)



Figure 48. Hybrid Servo Chain Assembly



Figure 49. 3-Phase Servo-Rotational Axis Magnetic Mount



CHAPTER 6: DISCUSSION AND FUTURE STUDIES

Method Development and Insights

Development and validation through clinical testing demonstrate the anthropometric utility of the simulator as a substitute for human studies. Automation of motion and simulated tissue may allow reproducible quantification of breast dynamics and bra-support influence. While breast dynamics vary among individuals, the 3D motion and tissue dynamics can change between them. This need to measure in 3D necessitates improved camera calibrations and use of more advanced DIC programs. While we use video cameras for motion capture, the need for simplification of quantification may benefit from other sensing modalities, e.g., larger arrays of pressure tubing sensors.

The formulations, molding, and overall structure of the simulator is important for function, usability, and for understanding bra apparel design-builds. The dynamics of surface-pressure-sensing and better anthropometric motion reproduction may provide a foundation for further study of breast motion and bra design. The current skin-tissue-lattice insertion/attachment structure also may allow for muscle and other organ structuring in the future. Overall durability of the simulator is also benefitted by replacement of tissue mass with tubing sensors while improving the durability of the skin simulant.

The molding techniques and composites used here may be applied to breast prosthetics. Beyond breast prosthetics and simulators, the tubing sensors may benefit prosthetic limb attachment; in addition to their sensing, they may be pressurized. Quantifying the connection

between the limb stump and the prosthetic sleeve may allow for monitoring and customization of fit and pressure for support of various activity levels and purposes.

The need to improve the original 3D scans to that of buoyant, neutral-position evaluation motivates future 3D scanning to occur underwater for better 3D scanning of breast tissue.

Future and Ongoing Studies

As part of NCSU IRB 14079, systems have been developed to 3D scan humans including a 3D ultrasound and surface scanners. Initial tests in the NCSU pool showed too many bubbles and turbulence for effective 3D ultrasound. As part of this study, both housings for surface scanning equipment, as well as a 3D ultrasound, were built.

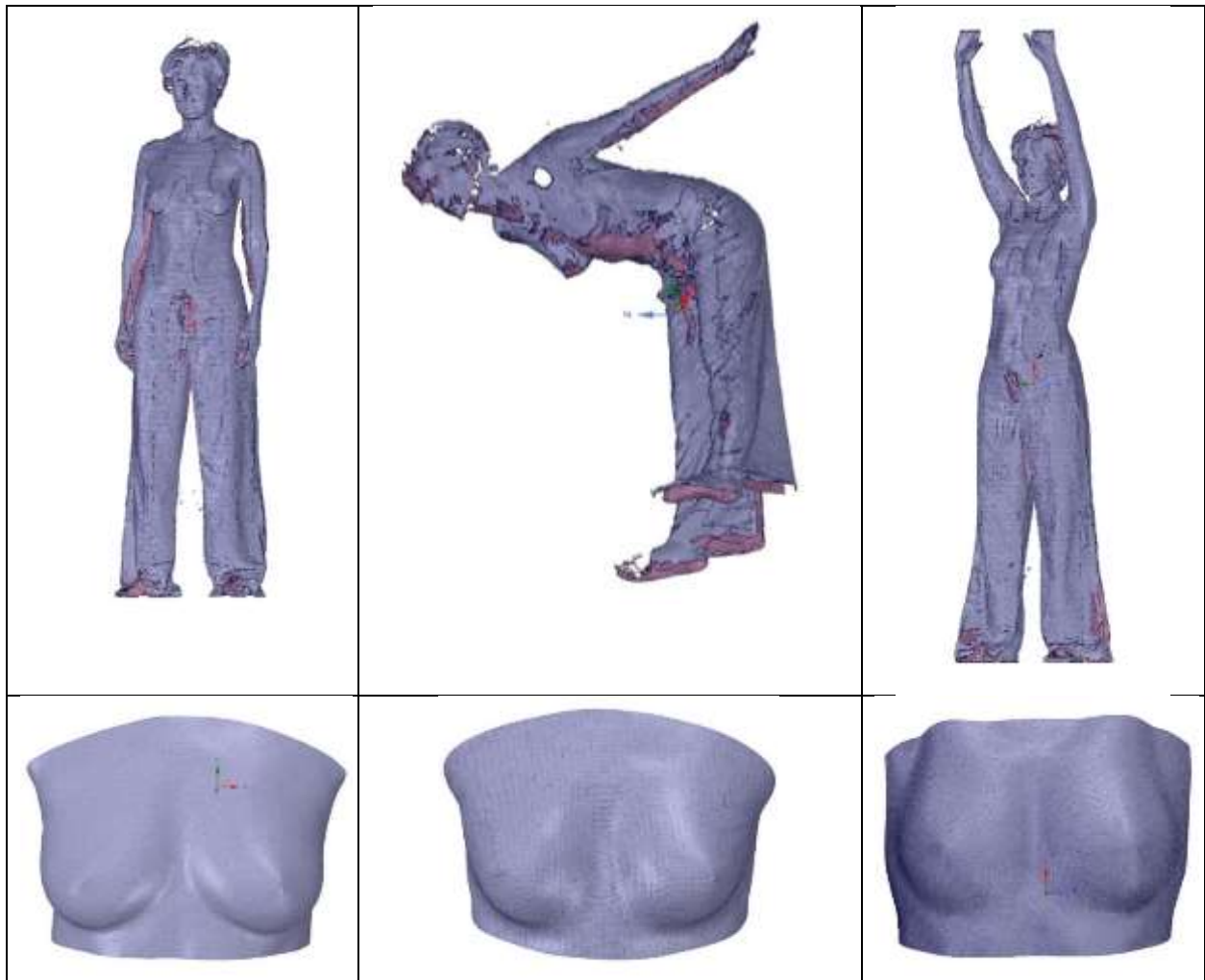
The 3D ultrasound consists of an XZY cantilever cartesian robot design built to traverse the C60e convex probe of the Sonosite Micromaxx Ultrasound system in the X direction. The stage is made from OpenBuilds Part Store using aluminum extrusion, plates, bearings, GT2 timing belt parts, and a m8 threaded rod (1.25mm pitch) with a corresponding Delrin nut on the Z axis plate. A probe holder was molded from Instamorph plastic to the C60e probe and then bolted to a piece of 20mmx20mm aluminum extrusion magnetically attached to the Y axis plate. The C60e probe is encased within a probe cover to allow it to go underwater. The C60e probe is in a sagittal position while the subject is vertical in the pool with only their head above the water. Starting laterally, the probe traverses the entirety of the breasts. The DICOM is recorded via both clips recording on the ultrasound itself and DVI output onto an external video recorder. In response to the bubble issue, a 180-gallon oval plastic tank was adapted into an underwater scanning chamber.

These underwater scanning techniques may, in the future, provide improved 3D scans not only for improved simulator reproduction, but also toward advancement of 3D human scans for









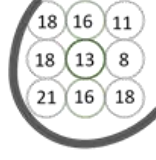
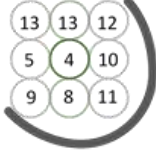



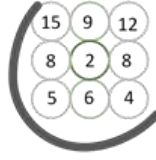
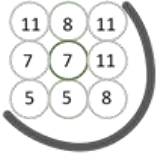
other medically related applications. Human reproduction may have application well beyond bra testing. By integrating anthropometric simulation and sensing into the simulator, additional benefit and ease of analysis may be developed in the future.

APPENDIX A

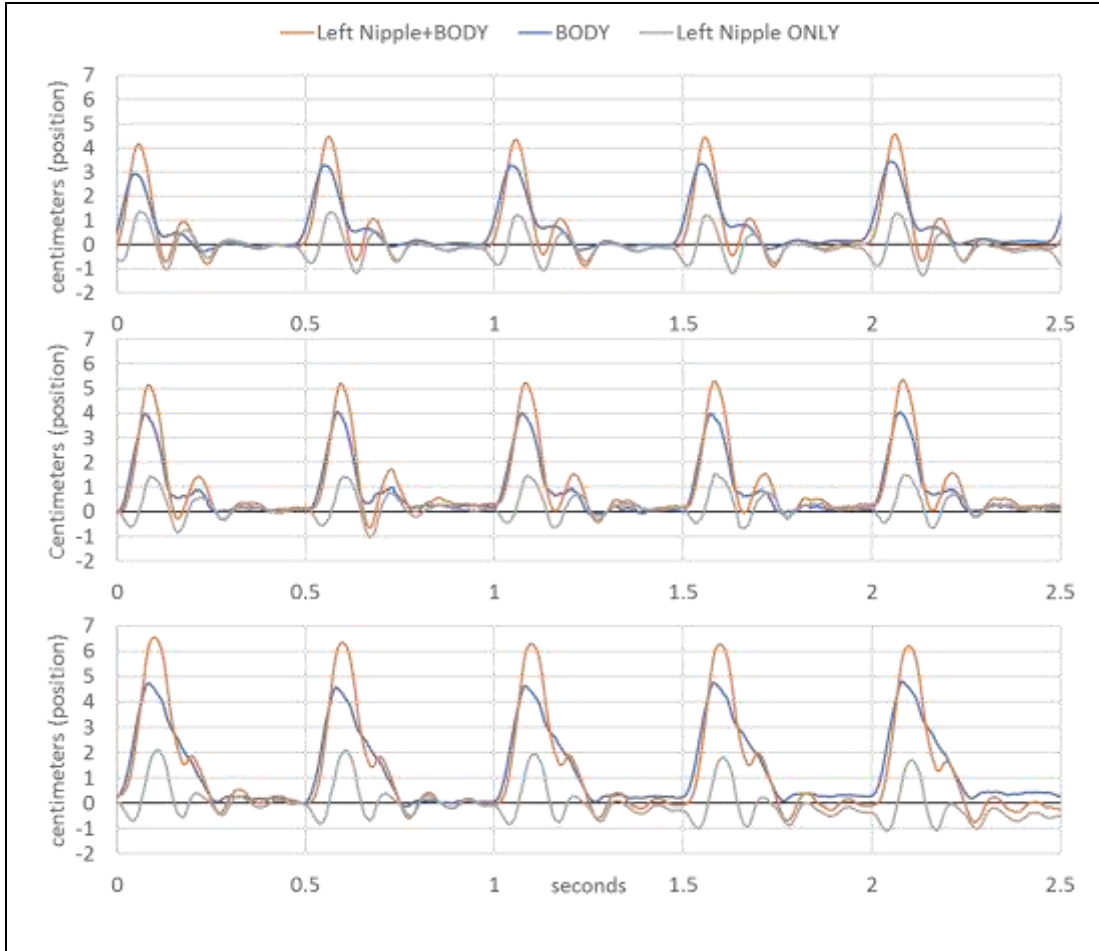
3D Scans in Various Positions (Upper: scan, Lower: breast mold)



Varying Position Simulator Durometer Data

<p>Standing scan</p> 			<div style="display: flex; justify-content: space-around;"> <div style="text-align: center;"> <p>AVG=26</p>  </div> <div style="text-align: center;"> <p>AVG=18</p>  </div> </div>
<p>Bend over scan</p> 			<div style="display: flex; justify-content: space-around;"> <div style="text-align: center;"> <p>AVG=15</p>  </div> <div style="text-align: center;"> <p>AVG=9</p>  </div> </div>
<p>Arms up scan</p> 			<div style="display: flex; justify-content: space-around;"> <div style="text-align: center;"> <p>AVG=8</p>  </div> <div style="text-align: center;"> <p>AVG=8</p>  </div> </div>

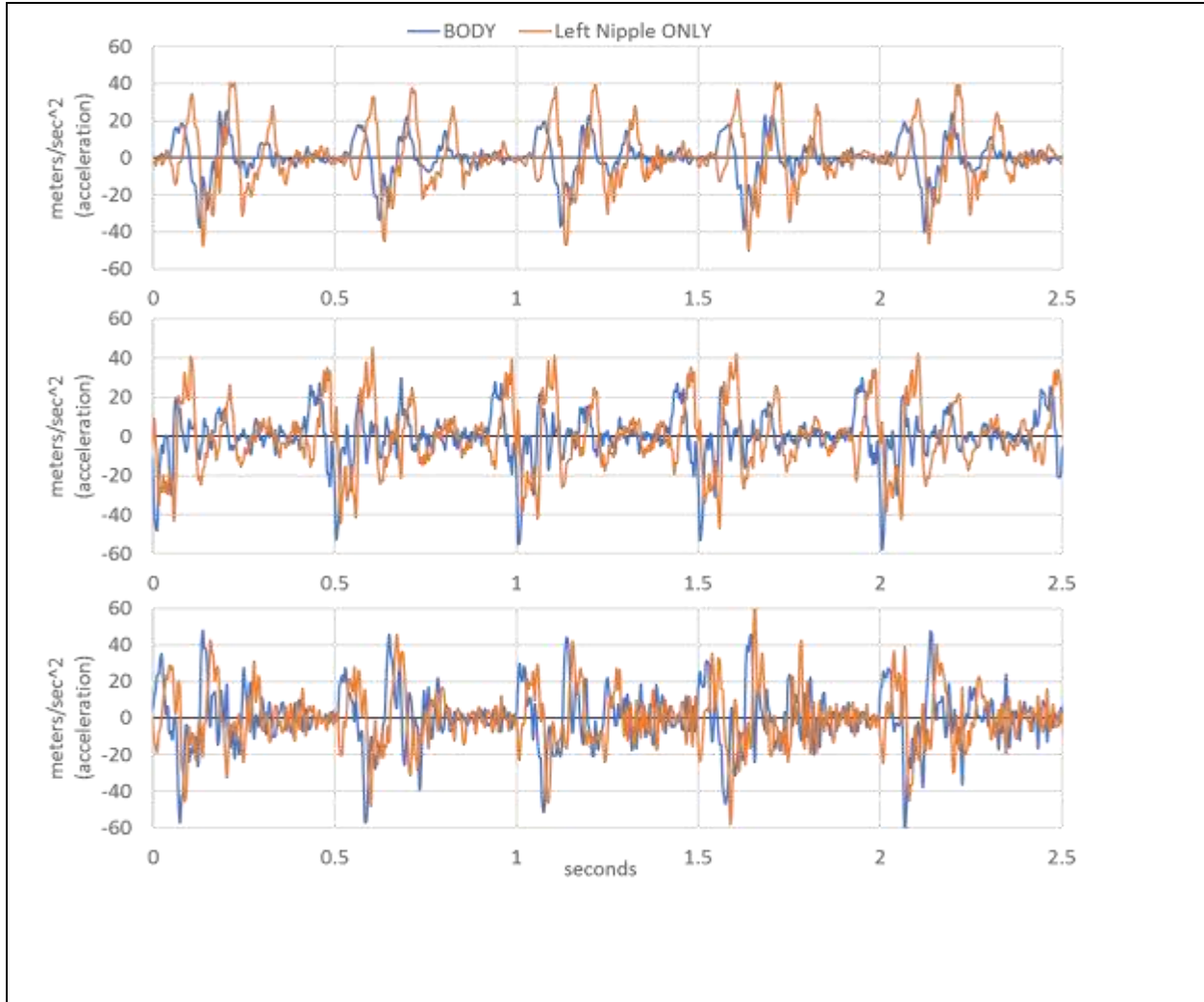
Varying Position Displacement Data



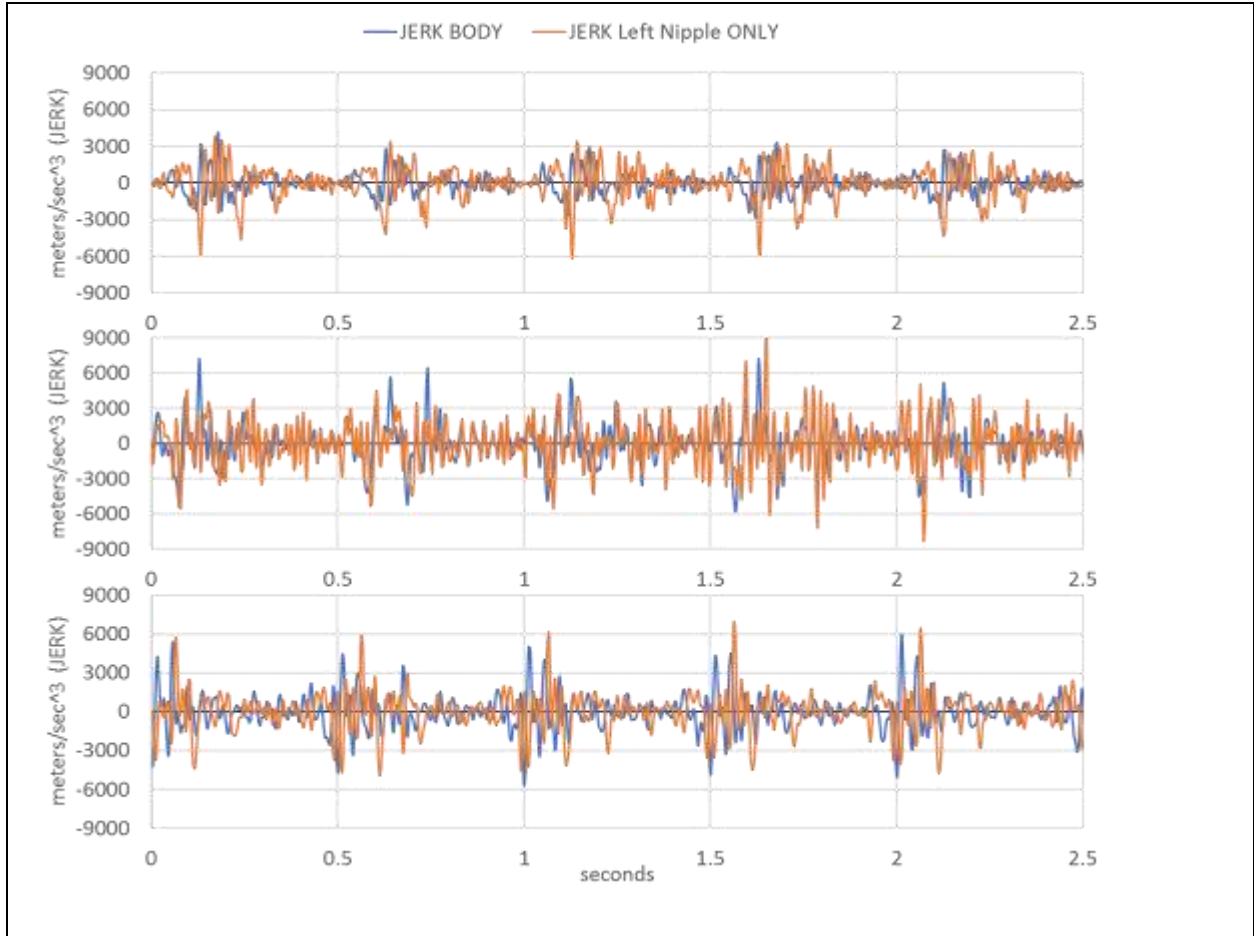
Varying Position Displacement Data

Vertical PEAK AVG (cm)	Vertical VALLEY AVG (cm)
1.16216	-1.25189
stdev	stdev
0.13249	0.13797
Ratio of (Max-Min) of Nipple ONLY to Body Motion	69.8%
Vertical PEAK AVG (cm)	Vertical VALLEY AVG (cm)
1.74871	-1.11633
stdev	stdev
0.24058	0.24058
Ratio of Total Nipple/BODY Acceleration	61.4%
Vertical PEAK AVG (cm)	Vertical VALLEY AVG (cm)
1.74871	-1.11633
stdev	stdev
0.24058	0.24058
Ratio of (Max-Min) of Nipple ONLY to Body Motion	61.4%

Varying Position Acceleration Data

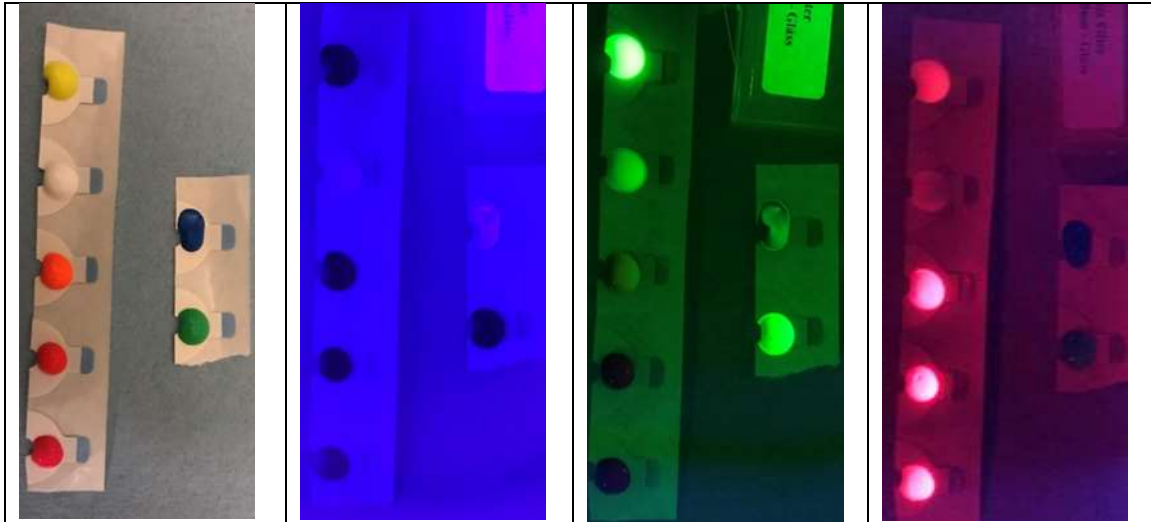


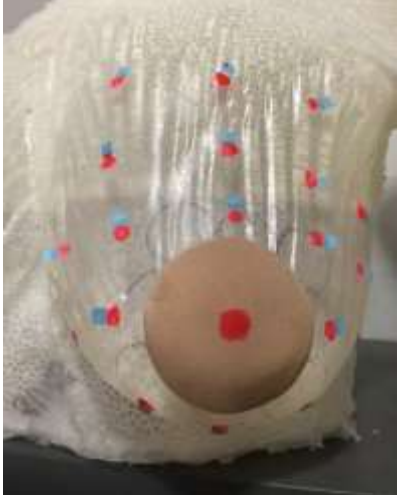
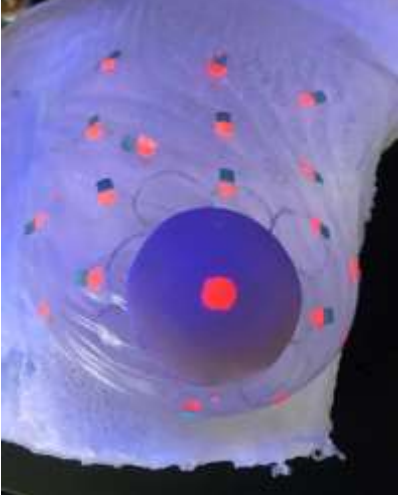

Varying Position JERK Data



APPENDIX B

Fluorescent Paint with Filters under Blacklight (ambient, blue, green, red filters)



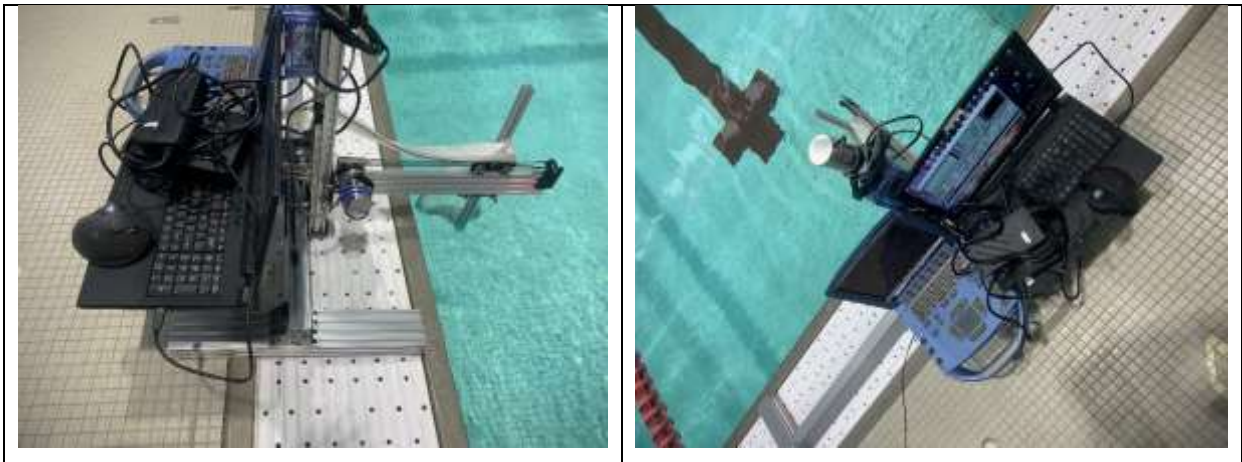
Breast with pastie and markers	Breast / markers under blacklight	Red filter used with blacklight
		

APPENDIX C

Underwater 3D Scanner and Camera Chamber



Underwater 3D Ultrasound



REFERENCES

- [1] d'Aulaire, Emily & d'Aulaire, Per Ola 1991-04-01, 'Mannequins: our fantasy figures of high fashion. (Cover Story)' *Smithsonian*, vol. v22, no. n1, pp. p66(11).
- [2] Simmons, K. P., & Istook, C. L. (2003). Body measurement techniques: Comparing 3D body-scanning and anthropometric methods for apparel applications. *Journal of Fashion Marketing and Management: An International Journal*, 7(3), 306-332.
- [3] Xu, T., Sheng, X., Zhang, T., Liu, H., Liang, X., & Ding, A. (2018). Development and validation of dummies and human models used in crash test. *Applied bionics and biomechanics*, 2018.
- [4] Baker, W. A., Untaroiu, C. D., Crawford, D. M., & Chowdhury, M. R. (2017). Mechanical characterization and finite element implementation of the soft materials used in a novel anthropometric test device for simulating underbody blast loading. *Journal of the mechanical behavior of biomedical materials*, 74, 358-364.
- [5] Seacrist, T., Balasubramanian, S., García-España, J. F., Maltese, M. R., Arbogast, K. B., Lopez-Valdes, F. J., ... & Higuchi, K. (2010, January). Kinematic comparison of pediatric human volunteers and the Hybrid III 6-year-old anthropomorphic test device. In *Annals of Advances in Automotive Medicine/Annual Scientific Conference (Vol. 54, p. 97)*. Association for the Advancement of Automotive Medicine.
- [6] Kuhlmann, M., Fear, E. C., Ramirez-serrano, A., & Federico, S. (2013). Medical Engineering & Physics Mechanical model of the breast for the prediction of deformation during imaging. *Medical Engineering and Physics*, 35(4), 470–478.

- [7] Griesenauer, R. H., Weis, J. A., Arlinghaus, L. R., Meszoely, I. M., & Miga, M. I. (2017). Breast tissue stiffness estimation for surgical guidance using gravity-induced excitation. *Physics in Medicine & Biology*, 62(12), 4756.
- [8] Rajagopal, V., Nash, M. P., Highnam, R. P., & Nielsen, P. M. F. (2008). The Breast Biomechanics Reference State for Multi-modal Image Analysis, 385–392.
- [9] Lee, A., Rajagopal, V., Chung, J., Bier, P., Nielsen, P. M. F., & Nash, M. P. (2008). Biomechanical Modelling for Breast Image Registration, 6918, 1–8.
- [10] Han, L., Hipwell, J. H., Tanner, C., Taylor, Z., Mertzaniidou, T., Cardoso, J., ... & Hawkes, D. J. (2011). Development of patient-specific biomechanical models for predicting large breast deformation. *Physics in Medicine & Biology*, 57(2), 455.
- [11] Gerling, G. J., Weissman, A. M., Thomas, G. W., & Dove, E. L. (2003). Effectiveness of a dynamic breast examination training model to improve clinical breast examination (CBE) skills, 27, 451–456.
- [12] Gerling GJ, Thomas GW. Augmented, pulsating tactile feedback facilitates simulator training of clinical breast examinations. *Hum Factors*. 2005;47:670-681.
- [13] Schubart, J. R., Erdahl, L., Smith, J. S., & Purichia, H. (2018). Use of Breast Simulators Compared with Standardized Patients in Teaching the Clinical. *JSURG*, 69(3), 416–422.
- [14] Davis, C. A., Mittura, K. L., Copeland, G. E., & Hawkins, E. M. (2011). Feasibility of a touch sensitive breast phantom for use in the training of physicians in clinical breast examination.
- [15] Tsimeris, J., Stevenson, D., Gedeon, T., & Adcock, M. (2013). Using ForceForm, a dynamically deformable interactive surface, for palpation simulation in medical scenarios.

Proceedings of the Second International Workshop on Smart Material Interfaces: Another Step to a Material Future - SMI '13, 19–22.

- [16] Govrin-Yehudain, J., Dvir, H., Preise, D., Govrin-Yehudain, O., & Govreen-Segal, D. (2015). Lightweight breast implants: a novel solution for breast augmentation and reconstruction mammoplasty. *Aesthetic surgery journal*, 35(8), 965-971.
- [17] Cruz, P., Hernandez, F., Zuñiga, M., Rodríguez, J., Figueroa, R., Vertiz, A., & Pineda, Z. (2018). A Biomimetic Approach for Designing a Full External Breast Prosthesis: Post-Mastectomy. *Applied Sciences*, 8(3), 357.
- [18] Jinde, L. (2009). Anatomy and clinical significance of the pectoral fascia. *Breast Augmentation: Principles and Practice*, 45–49.
- [19] Gefen, A., & Dilmoney, B. (2007). Mechanics of the normal woman's breast. *Technology and Health Care : Official Journal of the European Society for Engineering and Medicine*, 15(4), 259–271.
- [20] Adams Jr, W. P., & Mallucci, P. (2012). Breast augmentation. *Plastic and reconstructive surgery*, 130(4), 597e-611e.
- [21] Yu, W., Li, Y., Zheng, Y. P., Lim, N. Y., Lu, M. H., & Fan, J. (2006). Softness measurements for open-cell foam materials and human soft tissue. *Measurement Science and Technology*, 17(7), 1785–1791.
- [22] Mills, C., Sanchez, A., & Scurr, J. (2016). Estimating the gravity induced three dimensional deformation of the breast. *Journal of Biomechanics*, 49(16), 4134–4137.
- [23] Mills, C., Loveridge, A., Milligan, A., & Scurr, J. (2016). Trunk marker sets and the subsequent calculation of trunk and breast kinematics during treadmill running. *Textile Research Journal*, 86(11), 1128–1136.

- [24] Sanchez, A., Mills, C., Haake, S., Norris, M., & Scurr, J. (2017). Quantification of gravity-induced skin strain across the breast surface. *Clinical Biomechanics*, 50, 47-55.
- [25] Knight, M., Wheat, J., Driscoll, H., & Haake, S. (2014). A novel method to find the neutral position of the breast. *Procedia Engineering*, 72, 20-25.
- [26] Wang, C., & Wang, L. (2017). Comparison of breast motion at different levels of support during physical activity, 12(4), 1256–1264.
- [27] Peterson, A., & Suh, M. (2016). Effect of Bra Style and Size on its Fit and Comfort.
- [28] Coltman, C. E., McGhee, D. E., & Steele, J. R. (2015). Bra strap orientations and designs to minimise bra strap discomfort and pressure during sport and exercise in women with large breasts. *Sports medicine-open*, 1(1), 21.
- [29] Scurr, J., White, J., & Hedger, W. (2009). Breast displacement in three dimensions during the walking and running gait cycles. *Journal of Applied Biomechanics*, 25(4), 322–329.
- [30] White, J., Scurr, J., & Hedger, W. (2011). A Comparison of Three-Dimensional Breast Displacement and Breast Comfort During Overground and Treadmill Running, 47–53.
- [31] Milligan, A., Mills, C., & Scurr, J. (2014). Human Movement Science The effect of breast support on upper body muscle activity during 5 km treadmill running. *Human Movement Science*, 38, 74–83.
- [32] Haake, S., & Scurr, J. (2011). A method to estimate strain in the breast during exercise, 49–56.
- [33] Cai, Y., Chen, L., Yu, W., Zhou, J., Wan, F., Suh, M., & Chow, D. H. (2018). A piecewise mass-spring-damper model of the human breast. *Journal of Biomechanics*, 67, 137–143.
- [34] Haake, S., & Scurr, J. (2010). A dynamic model of the breast during exercise. *Sports Engineering*, 12(4), 189–197.

- [35] McGhee, D. E., Steele, J. R., Zealey, W. J., & Takacs, G. J. (2013). Bra e breast forces generated in women with large breasts while standing and during treadmill running : Implications for sports bra design. *Applied Ergonomics*, 44(1), 112–118.
- [36] Coltman, C. E., Steele, J. R., & McGhee, D. E. (2017). Effect of aging on breast skin thickness and elasticity: implications for breast support. *Skin Research and Technology*, 23(3), 303-311.
- [37] Busscher, I., Ploegmakers, J. J. W., Verkerke, G. J., & Veldhuizen, A. G. (2010). Comparative anatomical dimensions of the complete human and porcine spine, 1104–1114.
- [38] Dedieu, P., & Zanone, P. (2012). Human Movement Science Effects of gait pattern and arm swing on intergirdle coordination. *Human Movement Science*, 31(3), 660–671.
- [39] Egorov, V., & Sarvazyan, A. P. (2008). Mechanical imaging of the breast. *IEEE Transactions on Medical Imaging*, 27(9), 1275–1287.
- [40] Solav, D., Moerman, K. M., Jaeger, A. M., Genovese, K., & Herr, H. M. (2018). MultiDIC: An open-source toolbox for multi-view 3D digital image correlation. *IEEE Access*, 6, 30520–30535.
- [41] Xu, C., Wei, S., Xie, Y., Guan, X., Fu, N., Huang, P., & Yang, B. (2014). Combined use of the automated breast volume scanner and the US elastography for the differentiation of benign from malignant lesions of the breast. *BMC Cancer*, 14(1), 1–10.
- [42] Sigrist, R. M. S., Liao, J., Kaffas, A. El, Chammas, M. C., & Willmann, J. K. (2017). Ultrasound elastography: Review of techniques and clinical applications. *Theranostics*, 7(5), 1303–1329.

- [43] Sarvazyan, A., Hall, T. J., Urban, M. W., Fatemi, M., Aglyamov, S. R., & Garra, B. S. (2011). An overview of elasticity imaging - an emerging branch of medical imaging. *Current Medical Imaging Reviews*, 7(4), 255–282.
- [44] Haake, S., Milligan, A., & Scurr, J. (2012). Can measures of strain and acceleration be used to predict breast discomfort during running ?, 227(3), 209–216.
- [45] Grant, P. R., & Haycock, B. (2008). Effect of Jerk and Acceleration on the Perception of Motion Strength. *Journal of Aircraft*, 45(4), 1190-1197.